Supporting Information

Modulation of Charge Migration and Ink Flow Dynamics Exceeding 19% Efficiency for Blade-coating Pseudo-planar Heterojunction Organic Solar Cells

Houdong Mao, [a] Jiahua Zhang, [a] Xin Cen, [a] Jiayou Zhang, [b] Lin Wen, [a] Jingwei Xue, [d] Dou Luo,[e] Lifu Zhang, *[b] Zhao Qin, [a] Wei Ma, [d] Licheng Tan *[a], Yiwang Chen *[a,b,c]

[a]College of Chemistry and Chemical Engineering/Film Energy Chemistry for Jiangxi Provincial Key Laboratory (FEC), Nanchang University, 999 Xuefu Avenue, Nanchang 330031, China.
E-mail: tanlicheng@ncu.edu.cn (L. T); ywchen@ncu.edu.cn (Y. C.).
[b]Key Laborytary of Fluorine and Silicon for Energy Materials and Chemistry of Ministry of Education, Jiangxi Normal University, 99 Ziyang Avenue, Nanchang 330022, China.
E-mail: lifuzhang@jxnu.edu.cn (L. Z.)
[c]Peking University Yangtze Delta Institute of Optoelectronics, Nantong 226010, China
[d]State Key Laboratory for Mechanical Behavior of Materials School of Materials Science and Engineering Xi'an Jiaotong University, Xi'an 710049, China
[e]Department of Applied Biology and Chemical Technology and Research Institute for Smart Energy, The Hong Kong Polytechnic University, Hung Hom, Hong Kong, PR China

Experimental Section

Materials

Chemicals and solvents were obtained commercially and used without further purification unless stated otherwise. PM6, BTP-BO-4Cl, and PDINN were purchased from Solarmer Materials Inc., Ltd. Indium-tin oxide (ITO) glass was gained from South China Science & Technology Company Limited, whereas PEDOT: PSS (Clevios PVP Al4083) was obtained from J&K Scientific. Trimethoxy (1H,1H,2H,2H-heptadecafluorodecyl) silane (FAS, 98% purity) was purchased from Innochem. 1,3-dibromo-5-chlorobenzene (DBCl) was purchased from Sigma-Aldrich, and the ultra-dry toluene used in the experiments was obtained by redistillation. Silver (Ag) was obtained from Hebei JiuYue Advanced Material Technology Co., Ltd. The Si templates were purchased from Beijing Zhongke Jiming Technology Co., Ltd.

Devices fabrication

First, we generally choose to vacuum-plate an anti-sticking layer (heptadecafluoro-1, 1, 2, 2-tetrahydrodecyl-trimerhoxysilane, FAS) on the micropatterns template. Usually, the template is vacuum heated at 70 °C to deposit the anti-sticking layer. The conventional solar cell devices were fabricated with a structure of Glass/ITO/PEDOT: PSS/active layer/PDINN/Ag based on PM6/BO-4Cl and PM6/BO-4Cl: L8:BO systems. The ITO glass was cleaned by ultrasonic treatment in acetone, soap and deionized water, deionized water, isopropyl alcohol for 30 mins, respectively. Next, the ITO glass was treated 3 mins air plasma (Plasma Cleaner PPC862) after drying by Nitrogen gun. PEDOT: PSS (CLEVIOS P VP AI 4083) was spin-coated onto the ITO substrate at 4000 rpm for 1 min and PEDOT: PSS layer was annealed at 150 °C for 20 mins in ambient atmosphere. The coating of the active layer, it is divided into three

steps. First, the polymer PM6 (8 mg ml^{-1}) was blade-coated with a speed of 25 mm s^{-1} and the substrate temperature of 60 °C. The unimprinted PM6 films were annealed at 100 °C for 10 mins. Then imprinted PM6 films with different micropatterns at 150 °C and a certain pressure (3 MPa) in the vacuum on GD-nano-023. Subsequently, the system is cooled down while maintaining the applied pressure to prevent polymer donor reflowing. Finally, the template is released from the donor, and the donor nanograting with negative replication of the template is formed. Then, the acceptors BO-4Cl and BO-4Cl: L8-BO in TL (concentration: 9.6 mg ml^{-1}, 14 mg/ml DBCl) were blade-coated on the donor film under the same conditions and annealed at 100 °C for 10 mins. The PDINN (1 mg ml^{-1} in methyl alcohol) was deposited at 3000r s^{-1} at room temperature. Finally, 100 nm Ag layer was deposited as the top electrode under high vacuum (≈3 × 10^{-4} Pa) and the device was completed.

Instruments and Measurement

Optical characterizations: The *J-V* curves measurement was shown via the solar simulator (Enlitech, SS-F5-3A) along with AM 1.5G solar spectra whose light intensity was calibrated by the certified standard silicon solar cell (Enlitech, SK-2) at 100 mV cm^{-2}. UV-vis absorption spectra, the reflectance spectrum and the transmission spectrum were recorded on a Perkin Elmer Lambda 750 spectrophotometer. The steady-state photoluminescence (PL) spectra have been recorded by fluorescence spectrophotometer (Hitachi F-7000). Time-resolved photoluminescence (TRPL) has been measured by an Edinburgh Instruments FLS920.

X-ray diffraction (XRD) characterization: X-ray diffraction (XRD) micropatterns have been conducted by using Bruker D8Discover 25 X-ray diffractometer.

AFM and TEM characterizations:

TEM characterizations: First, we prepared PM6/BO-4Cl films imprinted with different micropatterns. We then cut the prepared film into an average of 80-100 pieces and place them in water, at which point the PEDOT:PSS will dissolve in the water and the film will fall off the substrate. We then place the copper mesh under the film, fish it and let it dry for testing.

The morphologies of active layers were investigated by Bruker Multimode8 high-resolution scanning probe microscope and a JEM-2010 HR microscope, respectively.

Scanning electron microscope (SEM): Scanning electron microscopy (SEM) has been conducted on SU8020 scanning electron microscope operated at an acceleration voltage of 5 kV.

Grazing Incidence Wide-Angle X-ray Scattering (GIWAXS) Characterization: GIWAXS measurements were performed at beamline 7.3.3 at the Advanced Light Source. Samples were prepared on Si substrates using identical blend solutions as those used in devices. The 10 keV X-ray beam was incident at a grazing angle of 0.11°-0.15°, selected to maximize the scattering intensity from the samples. The scattered x-rays were detected using a Dectris Pilatus 2M photon counting detector.

Finite element modeling analysis: The simulation used COMSOL Multiphisics software to construct the entire simulation, according to the model characteristics, using 3D components to construct data of several different microsurfaces, using the phase field two-phase flow method to simulate the coating process of local areas and fluids. where the laminar flow Navier-Stokes equation solves the velocity field. Its conservation equation is as follows:

$$\rho(u * \nabla)u = \nabla * [-pI + K] + F + \rho g$$

$$\nabla * (\rho u) = 0$$

Where ρ is the density (kg/ m^3), u is the velocity vector (m/s), p is pressure (Pa), I is the identity matrix, K is the viscous stress tensor (Pa), F is the volume force vector

(N/m^3), Cp is the specific heat capacity at constant pressure (J/(kg K)), T is the absolute temperature (K), q is the heat flux vector (W/m^2), Q contains the heat sources (W/m^3), S is the strin-rate tensor.

In the Phase Field interface, two-phase flow dynamics are controlled by the Cahn-Hilliard equation. This equation is used to track the diffusion interface of two incompatible liquids. The diffusion interface is defined as the region from -1 to 1 of dimensionless phase field variables. When solved in COMSOL Multiphysics, the Cahn-Hilliard equation is split into two equations:

$$\frac{\partial \emptyset}{\partial t} + u * \nabla \emptyset = \nabla * \frac{\gamma \lambda}{\varepsilon^2} \nabla \Psi$$

$$\Psi = -\nabla * \varepsilon^2 \nabla \emptyset + (\emptyset^2 - 1)\emptyset$$

where u is the fluid velocity (m/s), y is the mobility (m^3 s/kg), λ is the mixed energy density (N), ε (m) is the interface thickness parameter, Ψ variable is called the phase field helper. The following equation relates the mixed energy density and interfacial thickness to the surface tension coefficient:

$$\sigma = \frac{2\sqrt{2}\lambda}{3\varepsilon}$$

You can usually set the interface thickness parameter to = $h_c/2$, where h_c is the feature mesh size in the area through which the interface passes. The mobility parameter y determines the time scale of Cahn-Hilliard diffusion and must be chosen carefully. This parameter needs to be large enough to keep the interface thickness constant, and small enough to not over-suppress the convection term. The value y = is usually the initial valuation that applies. This model uses a higher mobility to obtain the correct pressure change at the interface.

FDTD theoretical simulations: The FDTD theoretical simulations were used to simulate the effect of grating structure on the light. The FDTD theoretical simulations

were performed by constructing an ideal model (Comsol, Hangzhou Yanqu Information Technology Co., Ltd.).

Surface energy characterization: Contact angle measurements of films were performed at a Krüss DSA100s Drop Shape Analyzer. Water (72.8 mN m-1, 25 °C) was used as probe liquid.

Dynamic X-ray photoelectron spectroscopy measurement: Dynamic X-ray photoelectron spectroscopy (DXPS, Thermo Scientific ESCALAB 250Xi) was used for binding energy and element distribution analysis.

Transient absorption (TA) spectroscopy measurement: For femtosecond transient absorption spectroscopy, the fundamental output from Yb: KGW laser (1030 nm, 220 fs Gaussian fit, 100 kHz, Light Conversion Ltd) was separated into two light beams. One was introduced to NOPA (ORPHEUS-N, Light Conversion Ltd) to produce a certain wavelength for pump beam (here we use 500 nm, 30 fs pulse duration), the other was focused onto a YAG plate to generate white light continuum as the probe beam. The pump and probe overlapped on the sample at a small angle of less than 10°. The transmitted probe light from the sample was collected by a linear CCD array.

FLIM measurement: Confocal photoluminescence (fluorescence) microscopy and lifetimes of photoluminescence (fluorescence) measurements (FLIM). The confocal PL microscopy and lifetimes of PL were detected by FastFLIM-Q2 by ISS (Champaign IIIinois, USA). The specimen for PL measurements was prepared using the same procedures for device preparation but without PDINO/Al on top of the active layer. For PL measurements, two (532 nm and 780 nm) lasers are pulsed at 20 MHz. The PL lifetime is obtained by single-exponential fitting.

Space-charge limited current (SCLC) measurements: The electron and hole mobility were measured by using the method of SCLC for electron-only devices with

the structure of ITO/ZnO/active layers/PDINN/Ag and hole-only devices with the structure of ITO/PEDOT: PSS/active layers/MoO_3/Ag. The fabrication conditions of the active layer films are same with those for the solar cells. The charge mobilities are generally described by the Mott-Gurney equation:

$$J = \frac{9}{8}\varepsilon_r\varepsilon_0\mu\frac{v^2}{L^3}$$

where J is the current density, ε_0 is the permittivity of free space (8.85×10^{-14} F/cm), ε_r is the dielectric constant of used materials, μ is the charge mobility, V is the applied voltage and L is the active layer thickness. The ε_r parameter is assumed to be 3, which is a typical value for organic materials. In organic materials, charge mobility is usually field dependent and can be described by the disorder formalism, typically varying with electric field, E=V/L, according to the equation:

$$\mu = \mu_0\exp\left[0.89\gamma\sqrt{\frac{V}{L}}\right]$$

Where μ_0 is the charge mobility at zero electric field and γ is a constant. Then, the Mott-Gurney equation can be described by:

$$J = \frac{9}{8}\varepsilon_r\varepsilon_0\mu_0\frac{V^2}{L^3}\exp\left[0.89\gamma\sqrt{\frac{V}{L}}\right]$$

In this case, the charge mobilities were estimated using the following equation:

$$\ln\left(\frac{JL^3}{V^2}\right) = 0.89\gamma\sqrt{\frac{V}{L}} + \ln\left(\frac{9}{8}\varepsilon_r\varepsilon_0\mu_0\right)$$

Trap-state density testing: The trap-state density was measured by the space charge limited current (SCLC) method. The electron-only device was fabricated by using structures of ITO/ZnO/active layer/PNDIT-F3N/Ag. The trap-state density was calculated with the equation in the trap-filled limit (TFL) region:

$$N_t = \frac{2\varepsilon_0 \varepsilon V_{TFL}}{eL^2}$$

Where N_t is the trap-state density, ε_0 is the permittivity of free space (8.85×10^{-12} F m^{-1}), ε_r is the relative permittivity of the material and L is the thickness of the active layer.

EQE_{EL} measurement: The highly sensitive EQE was measured by using an integrated system (Enlitech, PECT-600). The electroluminescence (EL) quantum efficiency (EQE_{EL}) measurements were performed by applying an external voltage/current source through the devices (Enlitech, REPS).

TPV and TPC measurement: TPV measurement was used to measure the lifetime of carriers. The background illumination was provided by a normal LED light source, and pulsed light was provided by arbitrary wave generator (AFG322C, Tektronix), eventually, the transient photovoltage signals for the device was collected by oscilloscope (MDO4104C, Tektronix).

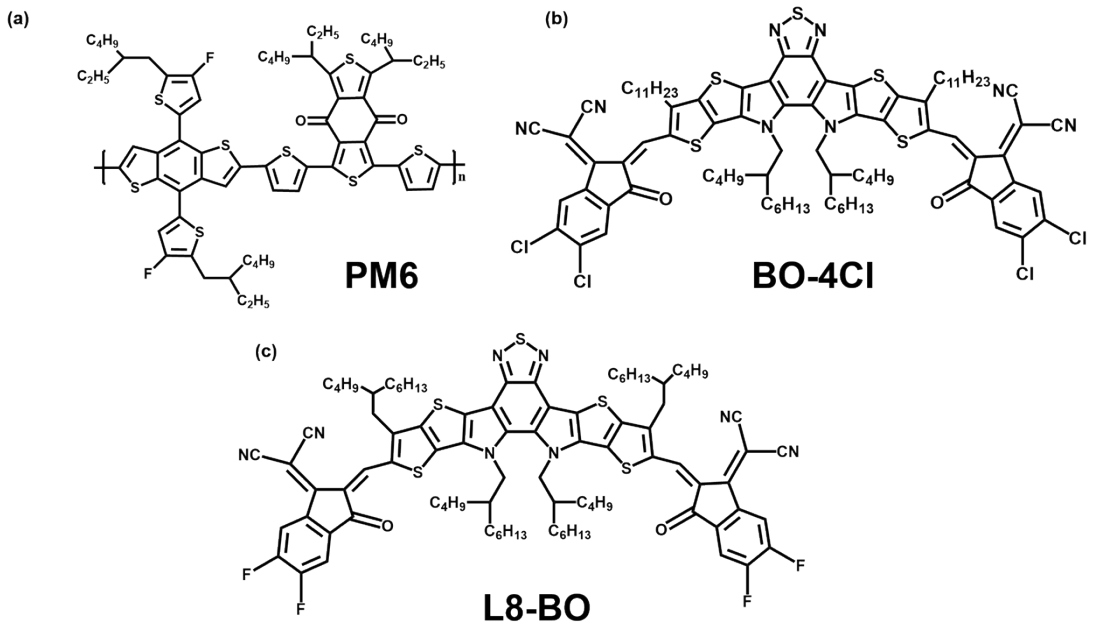

Figure S1. Chemical structures of (a) polymer donor PM6, small molecular non-fullerene acceptors (b) BO-4Cl and c) L8-BO.

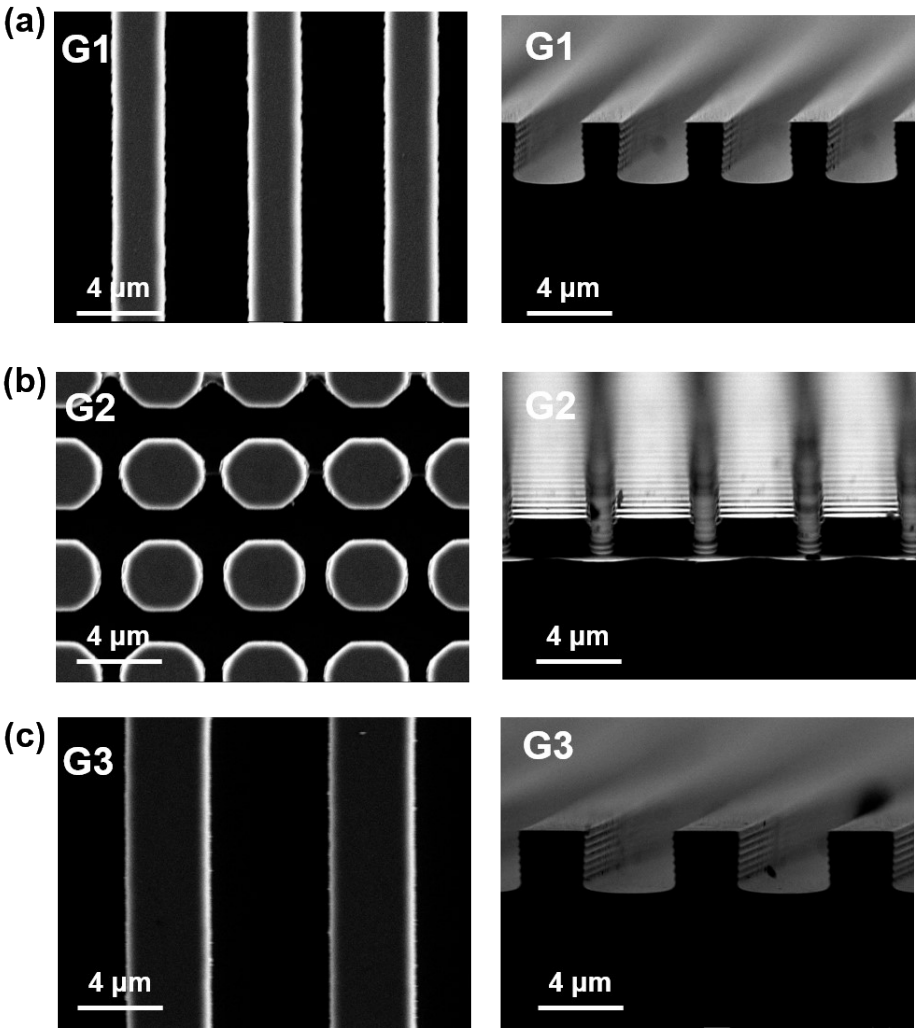

Figure S2. Planar scanning electron microscopy (SEM) and cross-sectional SEM images of (a) G1 (grating; the width, depth and pitch are 2 μm), (b) G2 (cylindrical; the width, depth and pitch are 2 μm), and (c) G3 (grating, the width and pitch are 3 μm while the depth is 2 μm).

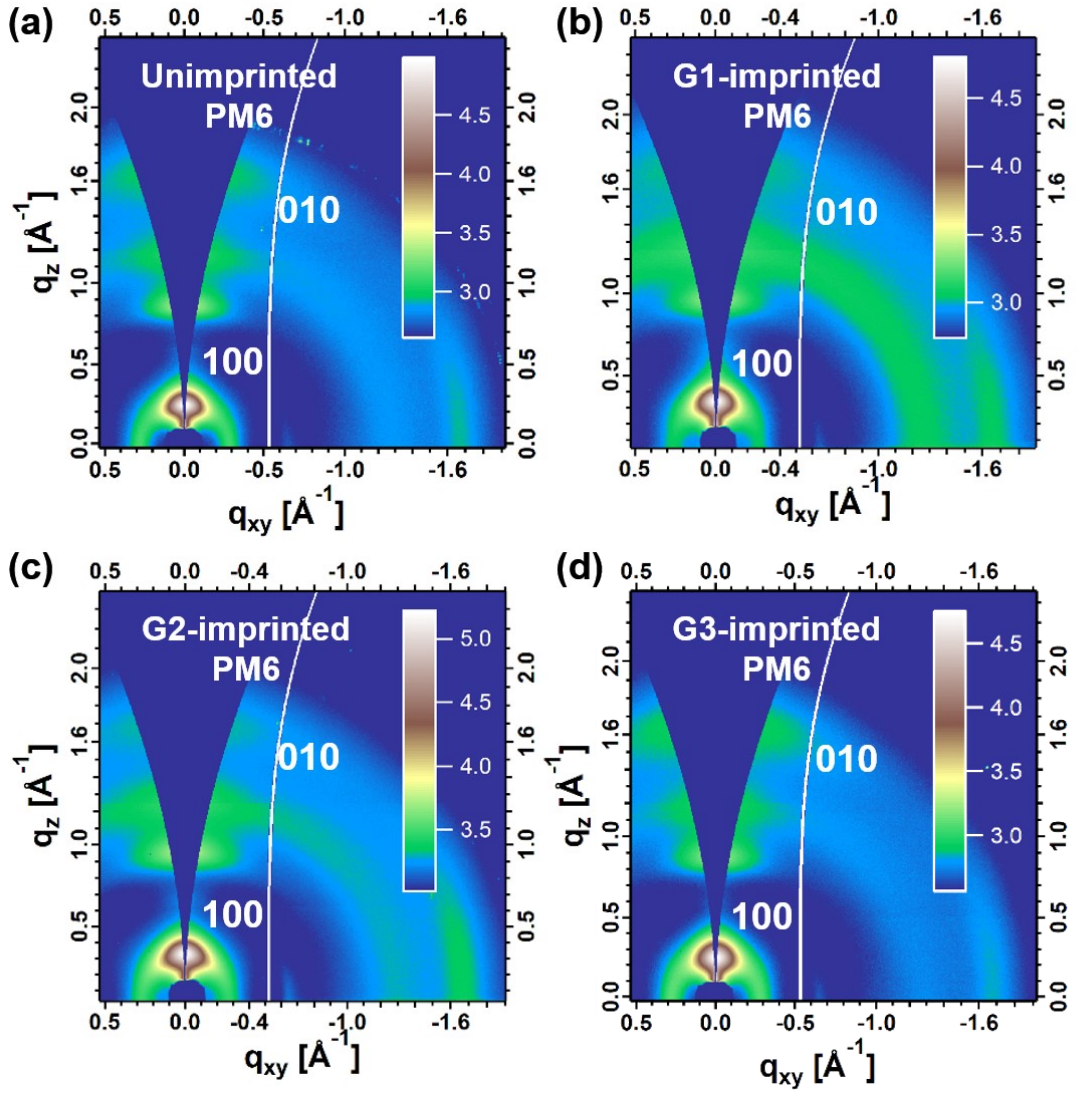

Figure S3. (a-d) Grazing incidence wide-angle X-ray scattering (GIWAXS) 2D scattering patterns of unimprinted and imprinted PM6 films with different micropatterns.

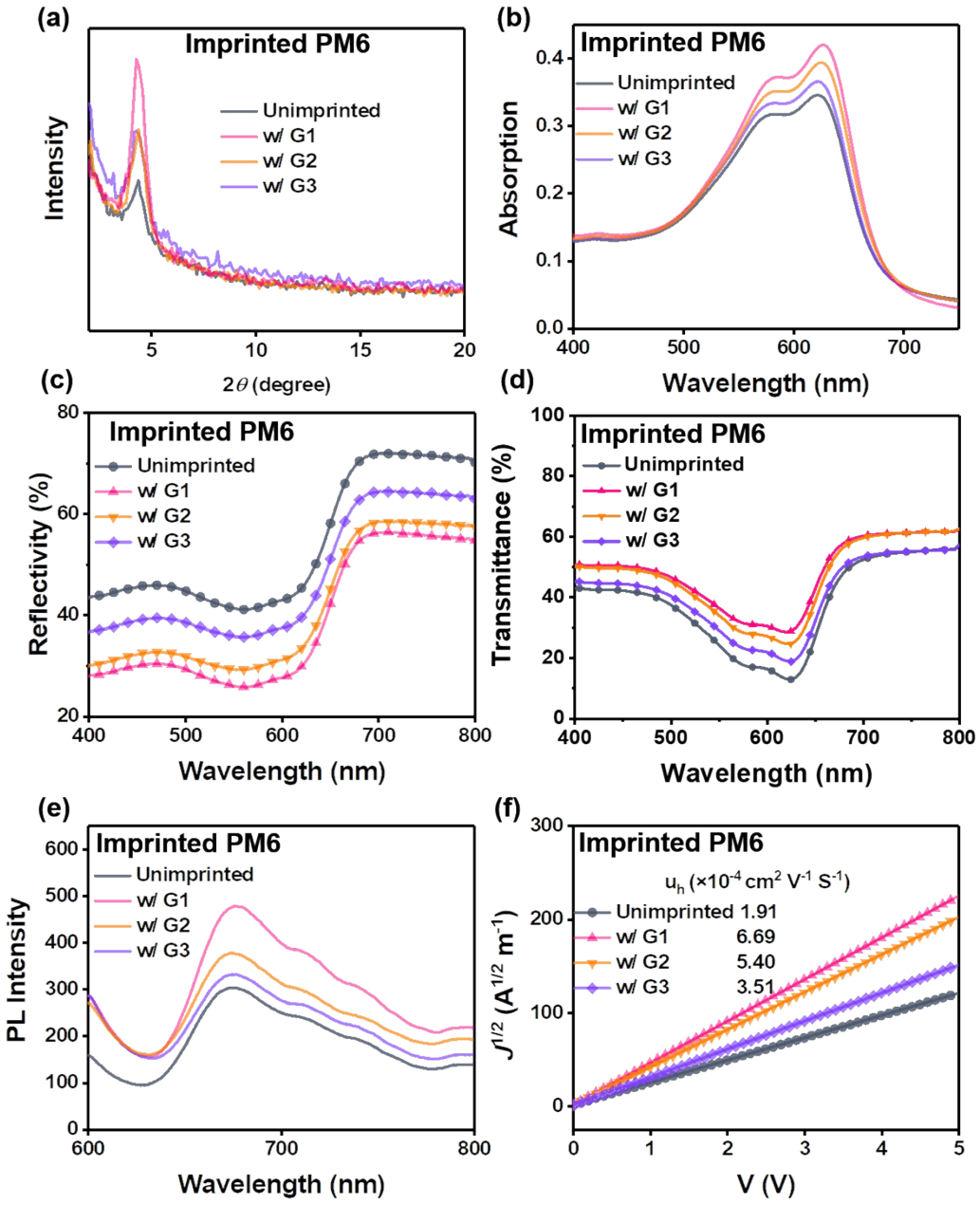

Figure S4. (a) X-ray diffraction (XRD) patterns, (b) UV-vis absorption spectra, (c) reflectivity spectra, (d) transmittance spevtra, (e) steady-state photoluminescence (PL) spectra of unimprinted and imprinted PM6 films with different micropatterns. (f) Dark *J-V* curves of the hole-only devices with the structure of ITO/PEDOT:PSS/PM6 films (unimprinted and imprinted with different micropatterns)/MoO_3/Ag based on the space-charge limited current (SCLC) model.

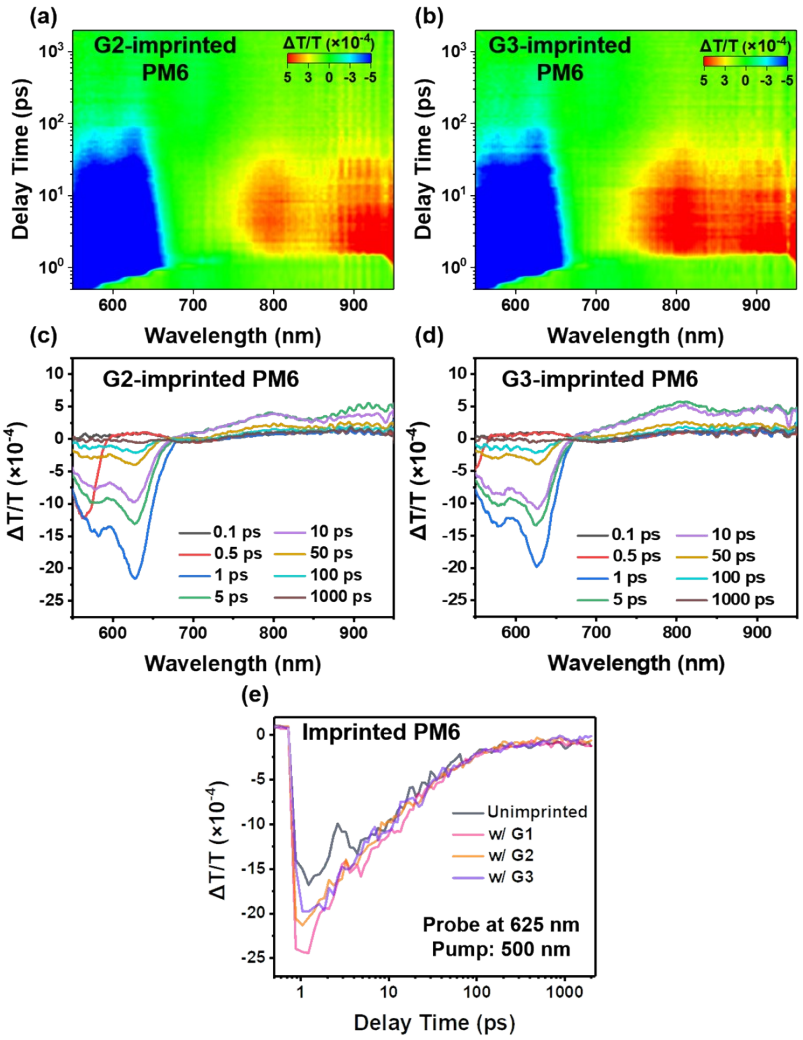

Figure S5. (a, b) Transient absorption (TA) spectra and (c, d) the corresponding TA spectra recorded at different delay times of G2-imprinted and G3-imprinted PM6 films. (e) The dynamic curves of TA results at 625 nm of unimprinted and imprinted PM6 films with different micropatterns.

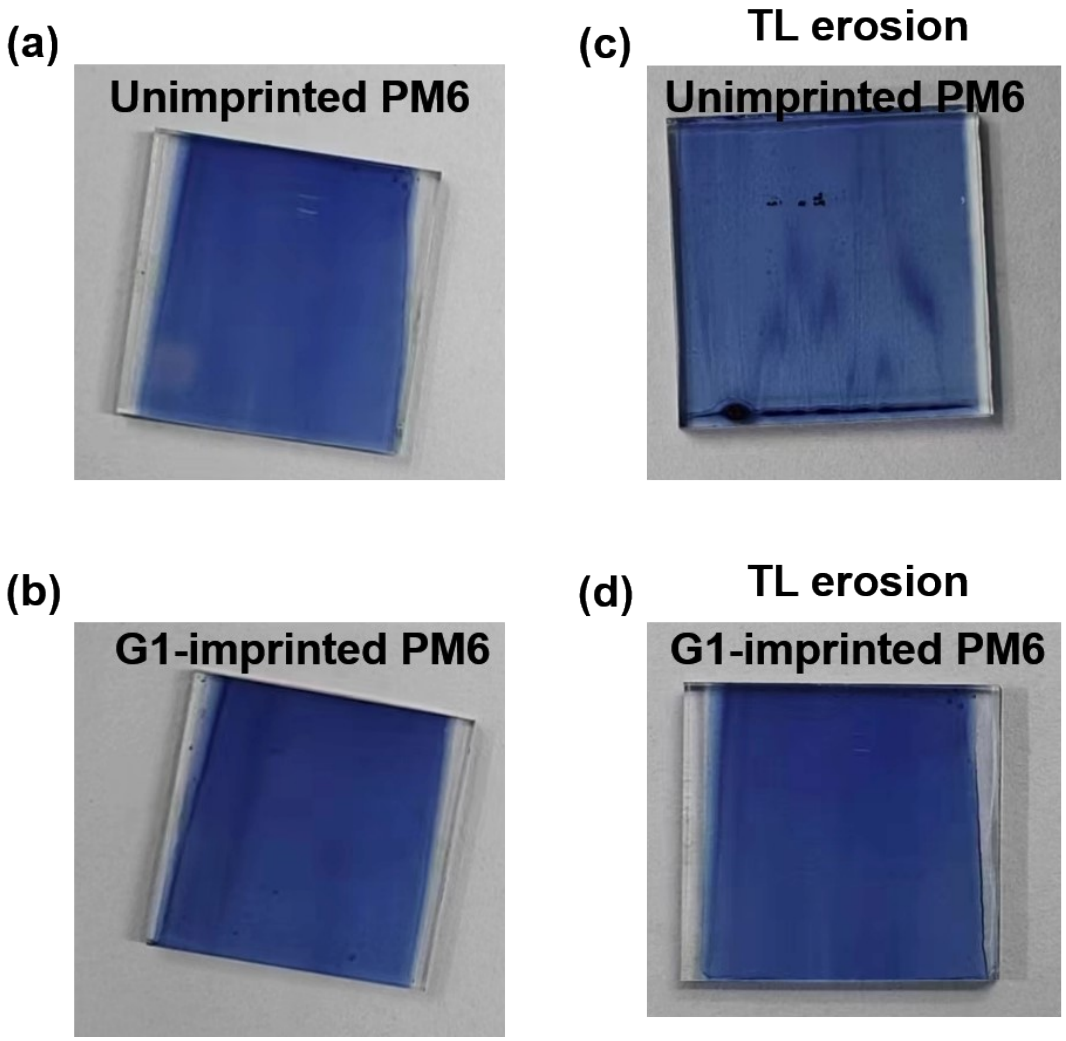

Figure S6. (a, b) The PM6 films of unimprinted and G1-imprinted. (c, d) The PM6 films of unimprinted and G1-imprinted after TL erosion.

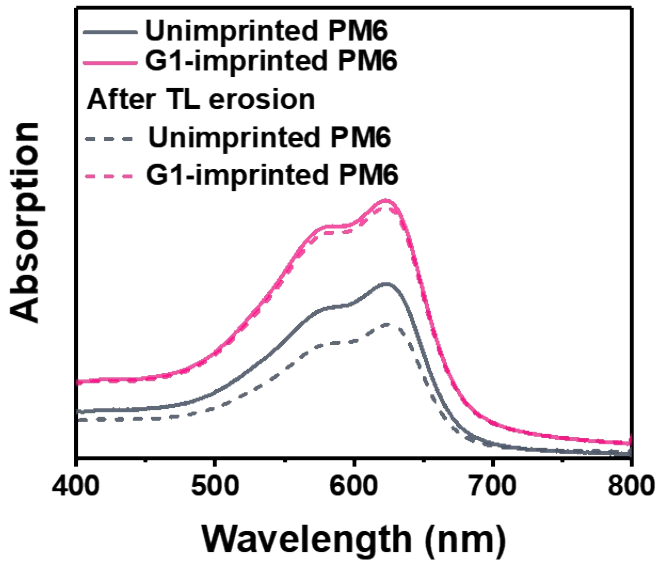

Figure S7 UV-Vis absorption spectra for the unimprinted and G1-imprinted PM6 via toluene (TL) solution erosion.

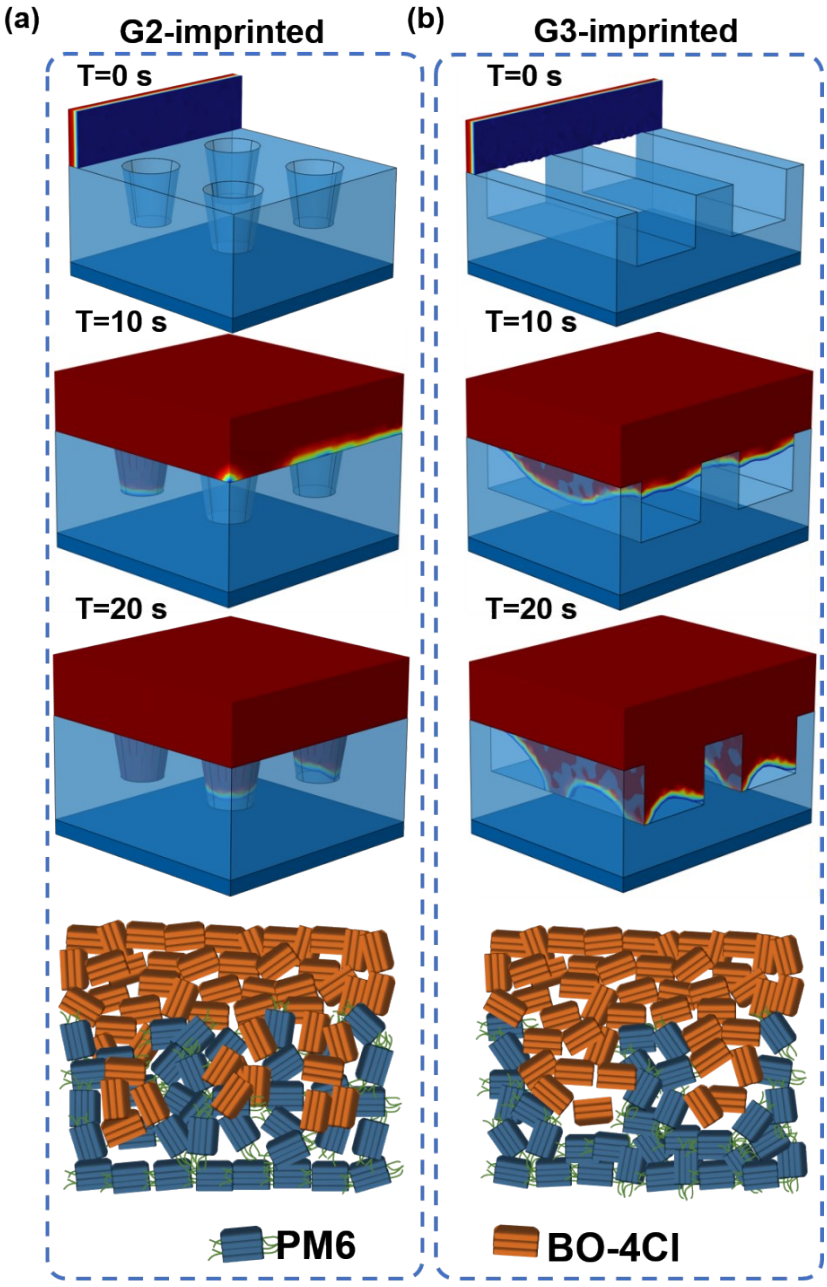

Figure S8. The filling degree of acceptor in the imprinted donor as a function of blade coating time, and schematic diagram of the vertical composition evolution of PM6/BO-4Cl films based on (a) G2-imprinted PM6, and (b) G3-imprinted PM6.

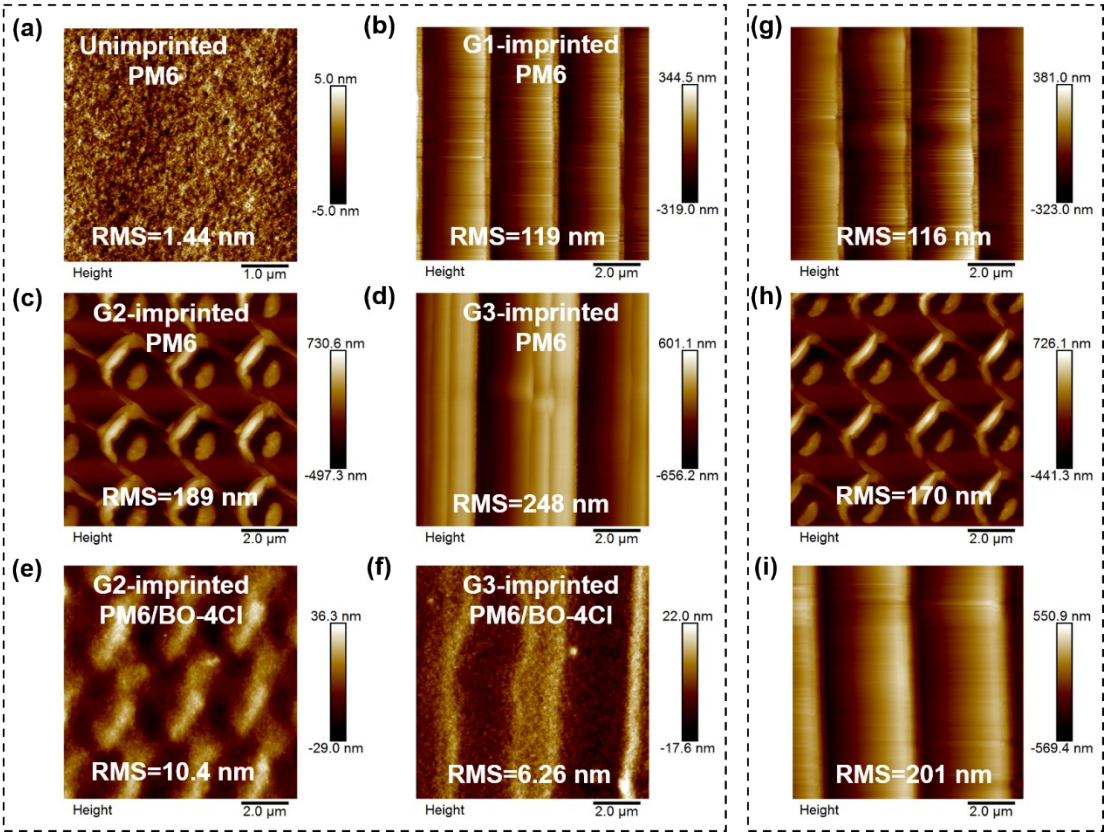

Figure S9. Atomic force microscopy (AFM) images of (a-d) unimprinted and imprinted PM6 films with different micropatterns, (e) G2-imprinted PM6/BO-4Cl and (f) G3-imprinted PM6/BO-4Cl. (g-i) The AFM images after TL esosion of imorinted with different micropatterns.

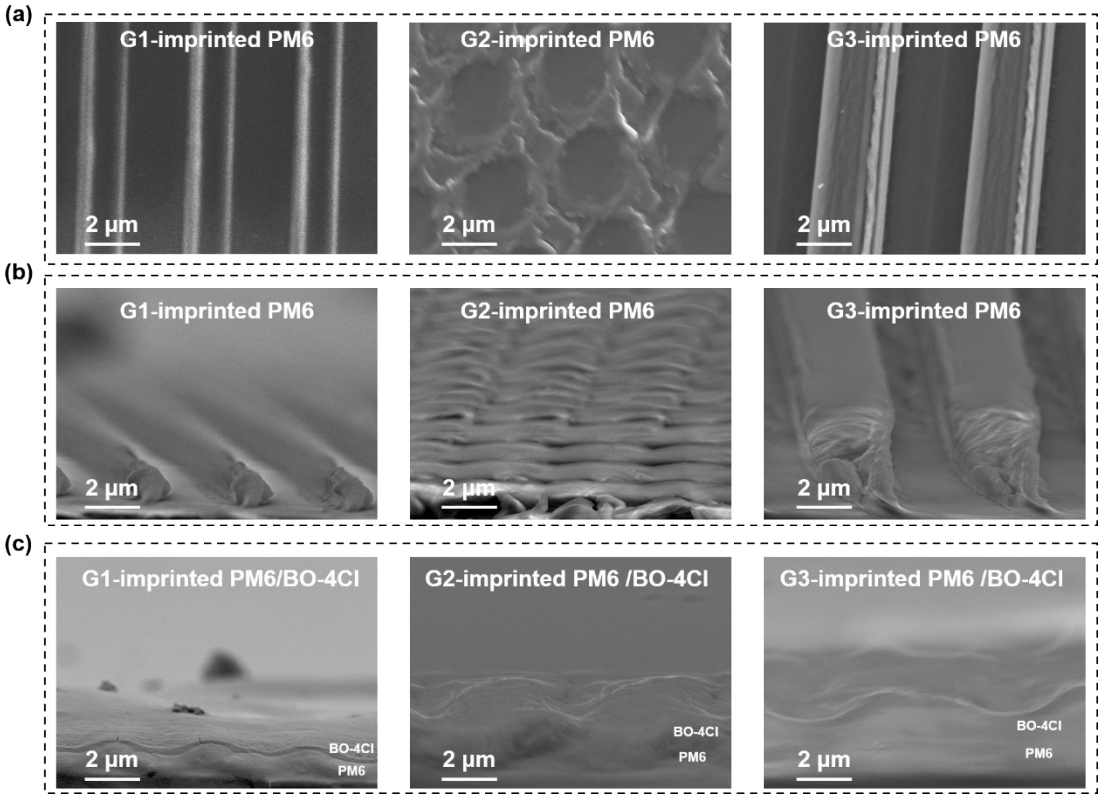

Figure S10. a) Planar and b) cross-sectional SEM images of imprinted PM6 and c) cross-sectional SEM image of imprinted PM6/BO-4Cl with different micropatterns.

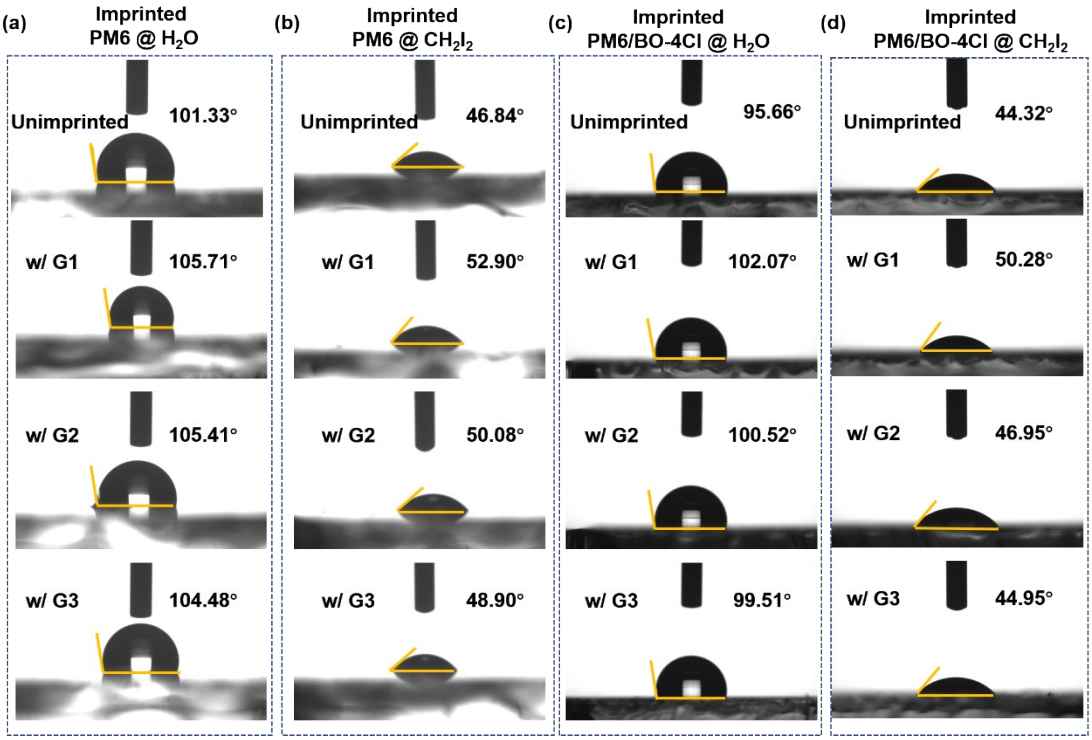

Figure S11. The contact angles of H_2O and CH_2I_2 of unimprinted and imprinted (a, b) PM6, and (c, d) PM6/BO-4Cl films with different micropatterns.

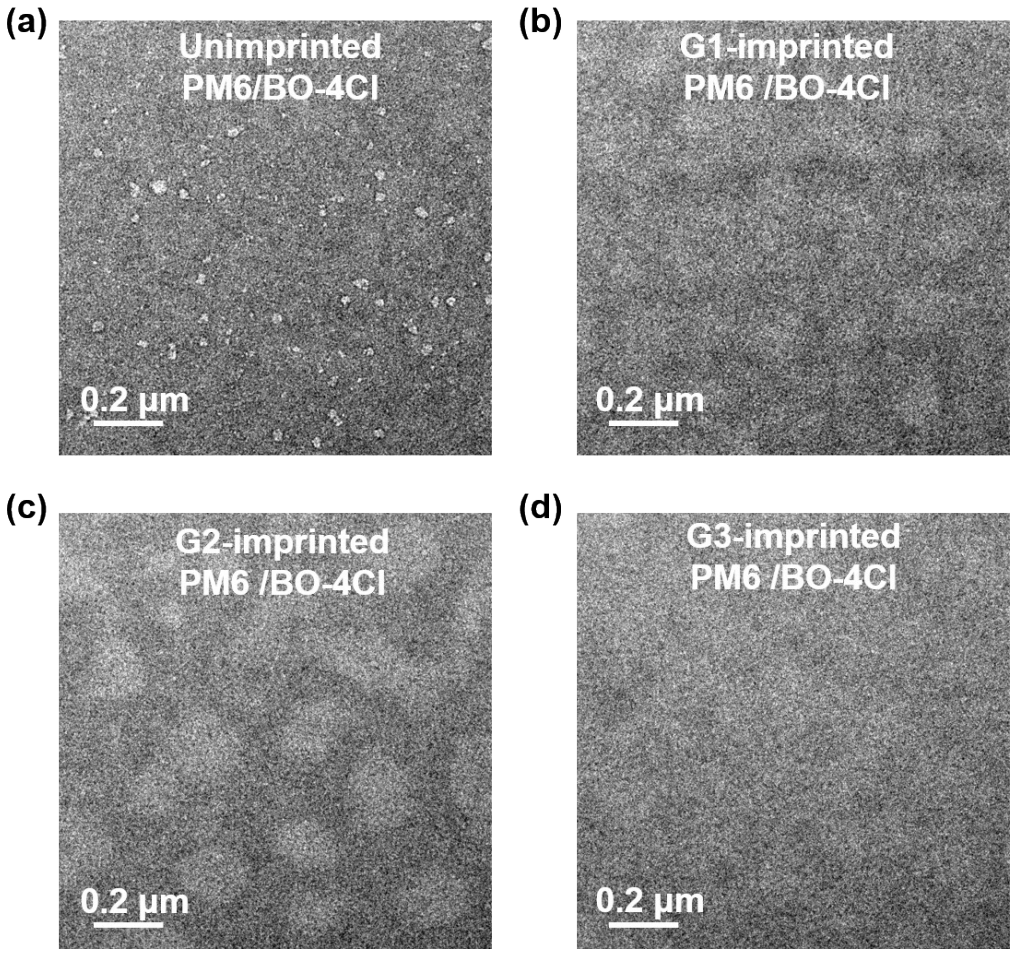

Figure S12. Transmission electron microscopy (TEM) images of unimprinted and imprinted PM6/BO-4Cl films with different micropatterns.

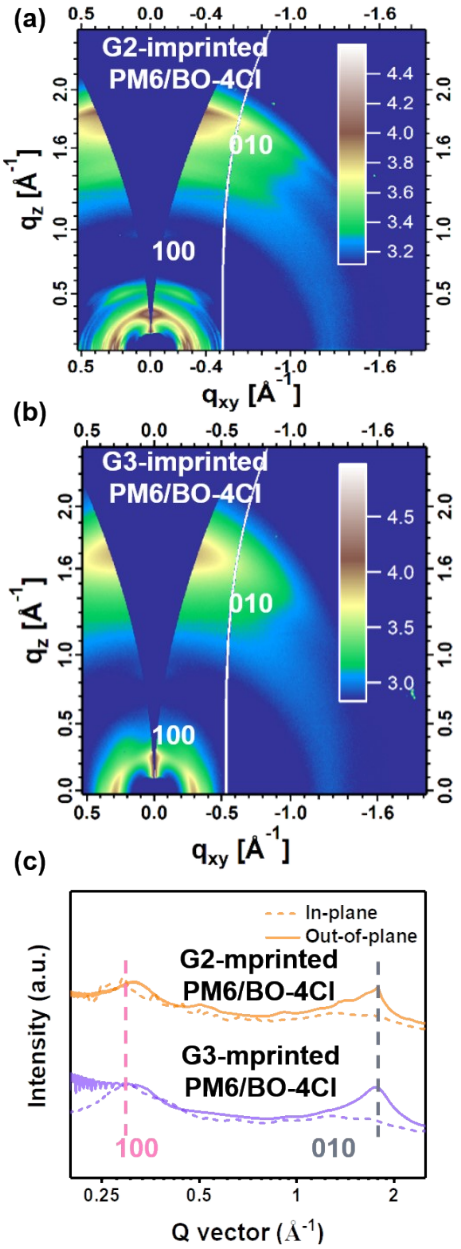

Figure S13. (a, b) GIWAXS 2D scattering patterns, and (c) 1D lines profiles of PM6/BO-4Cl films based on G2-imprinted PM6 and G3-imprinted PM6.

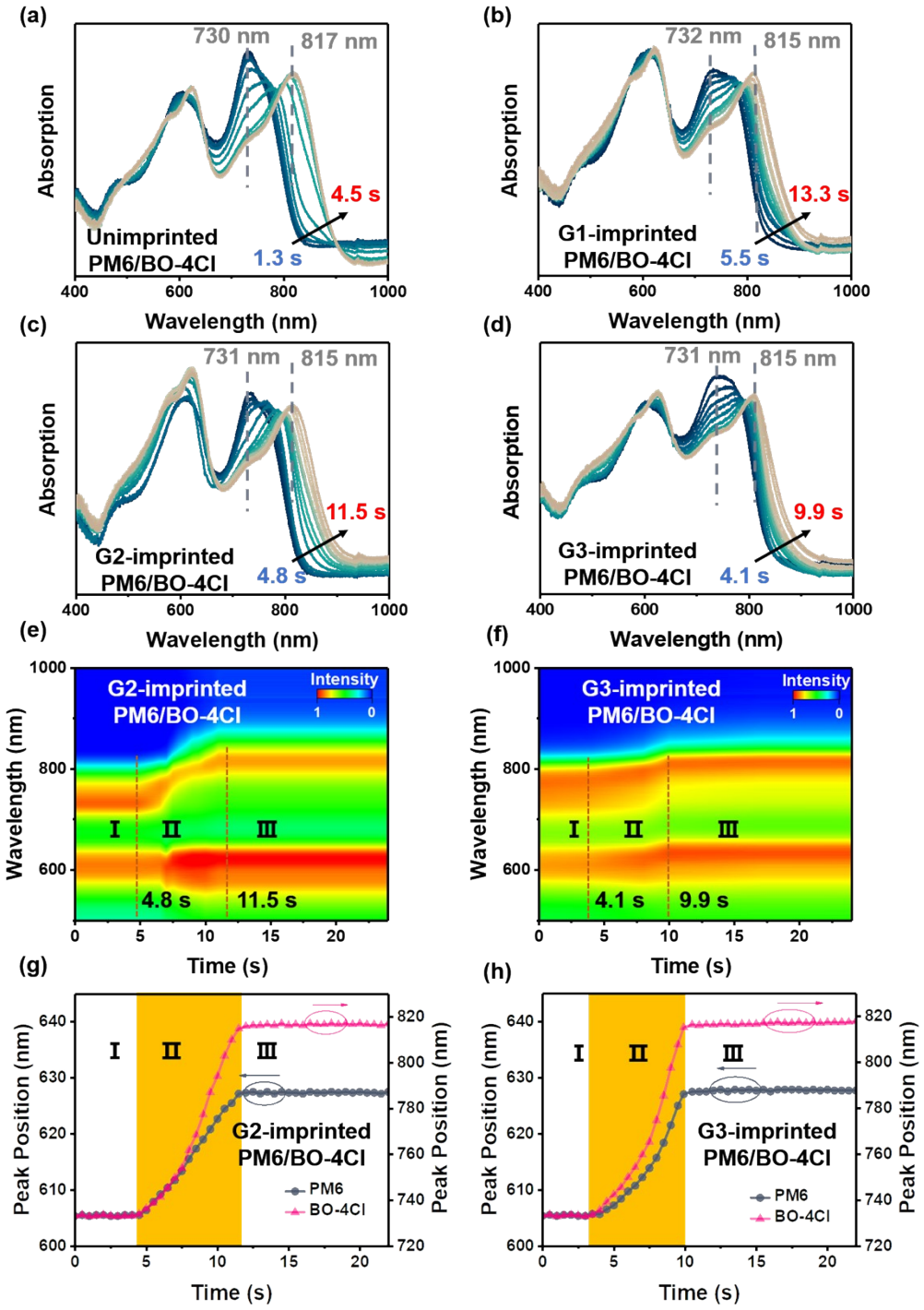

Figure S14. (a-d) In situ UV-vis absorption line profiles of unimprinted and imprinted PM6/BO-4Cl films with different micropatterns. (e, f) Time-resolved UV-vis absorption spectra and (g, h) peak position evolution as a function of time for PM6/BO-4Cl films with G2-imprinted PM6 and G3-imprinted PM6.

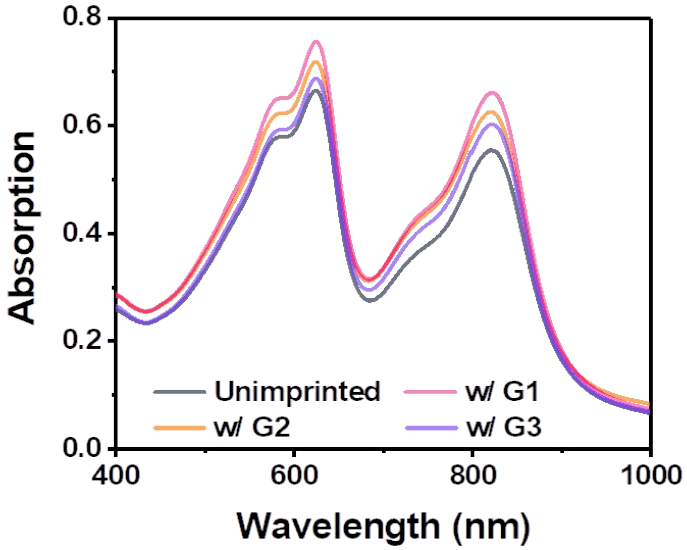

Figure S15. UV-vis absorption spectra of unimprinted and imprinted PM6/BO-4Cl films with different micropatterns.

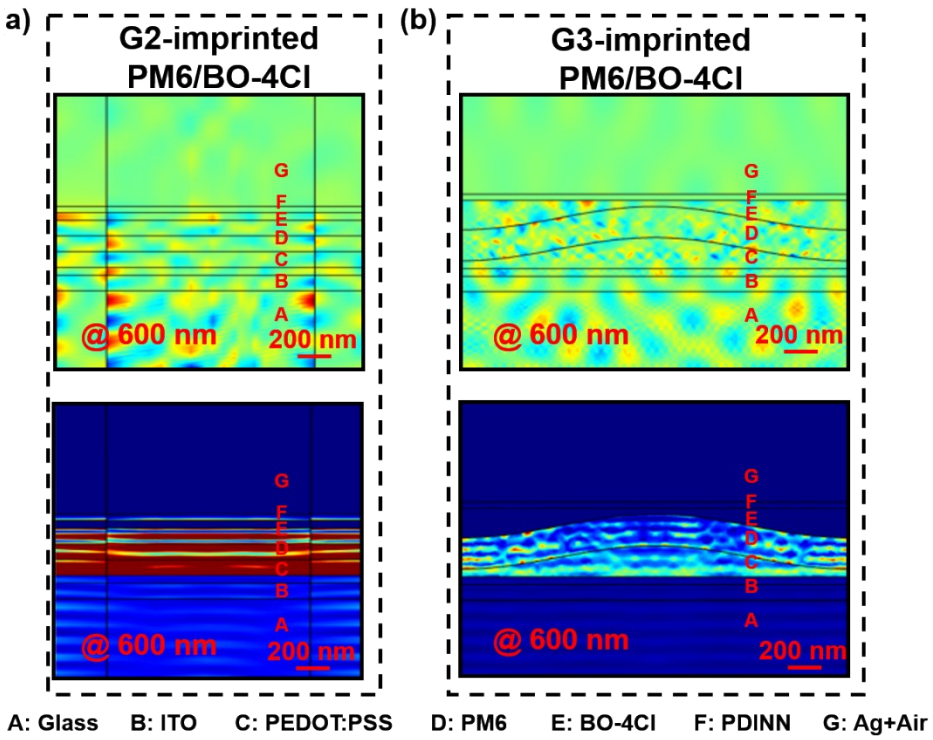

Figure S16. Simulated electric field (Ey) distribution maps and simulated absorption maps (under 600 nm illumination) of PPHJ OSCs based on (a) G2-imprinted PM6, and (b) G3-imprinted PM6.

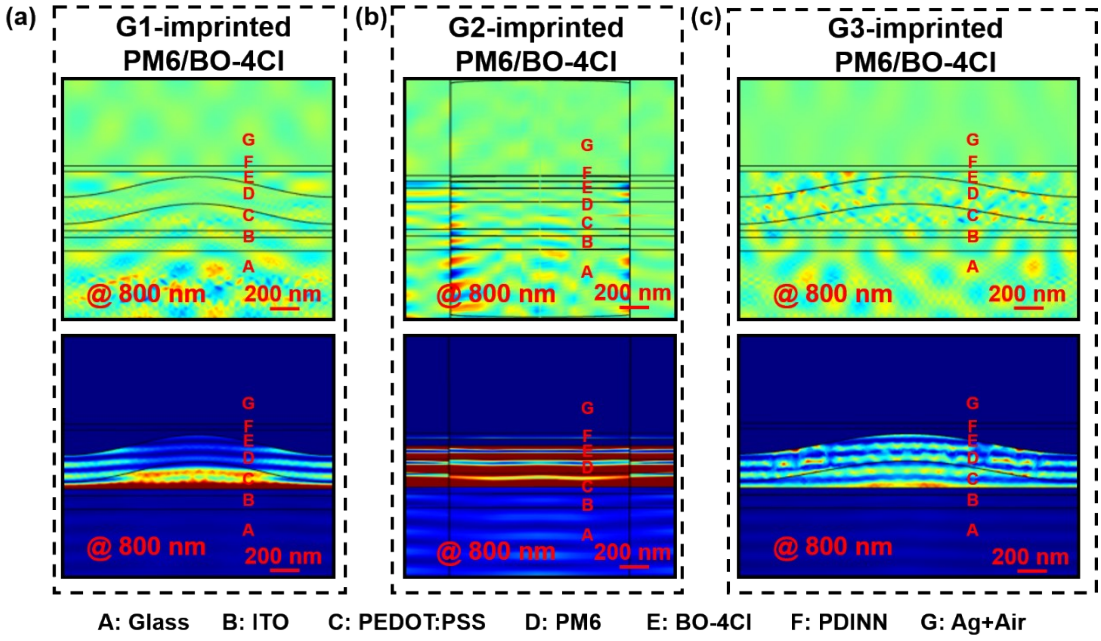

Figure S17. Simulated electric field (Ey) distribution maps and simulated absorption maps (under 800 nm illumination) of PPHJ OSCs based on (a) G1-imprinted PM6, (b) G2-imprinted PM6, and (c) G3-imprinted PM6, respectively.

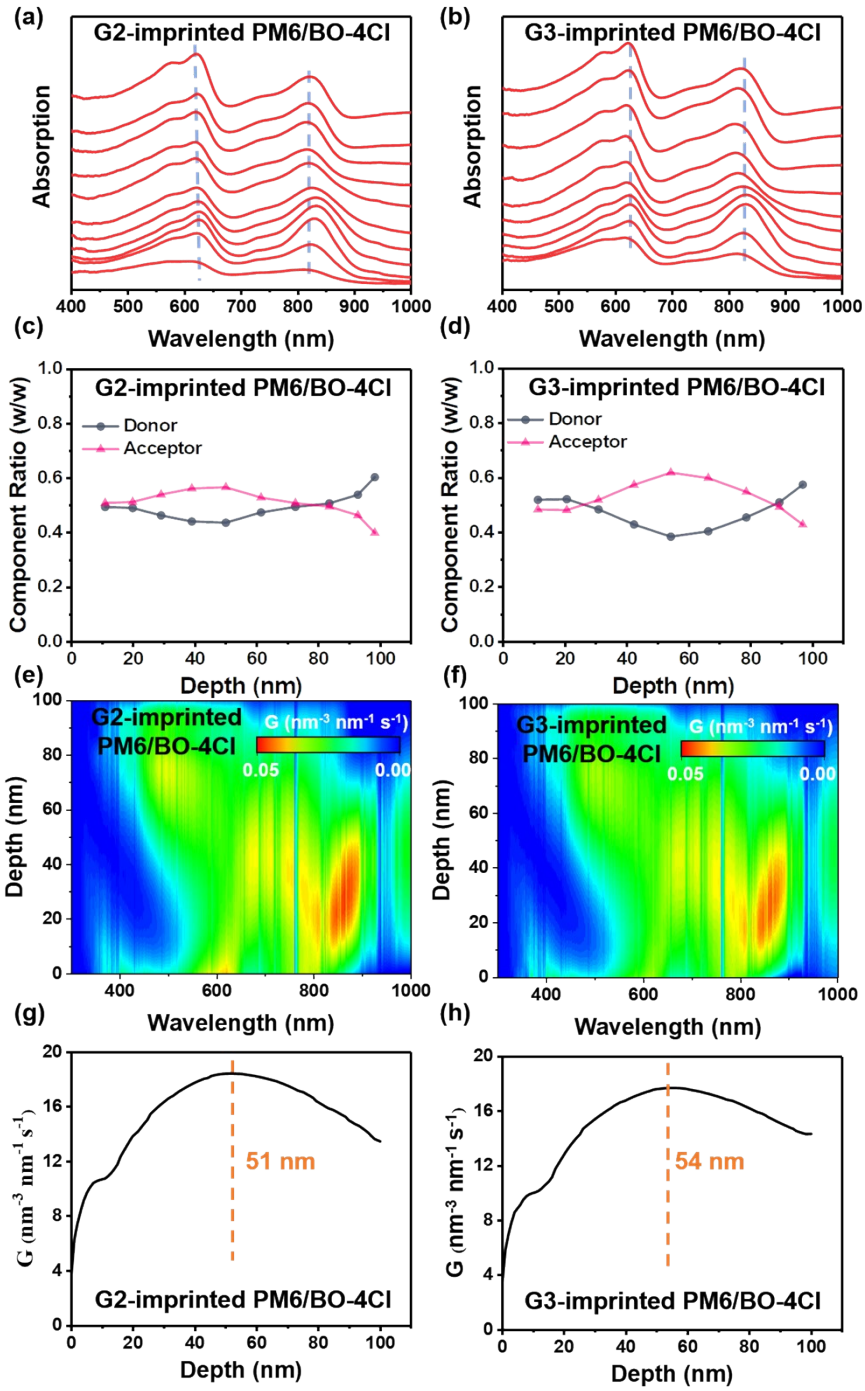

Figure S18. (a, b) Film-depth-dependent light absorption spectra, (c, d) film-depth-dependent composition profiles, (e, f) exciton generation contours, and (g, h) the dependence of the simulated exciton generation rates at each wavelength as a function of the film thickness of PM6/BO-4Cl films with G2-imprinted PM6 and G3-imprinted PM6.

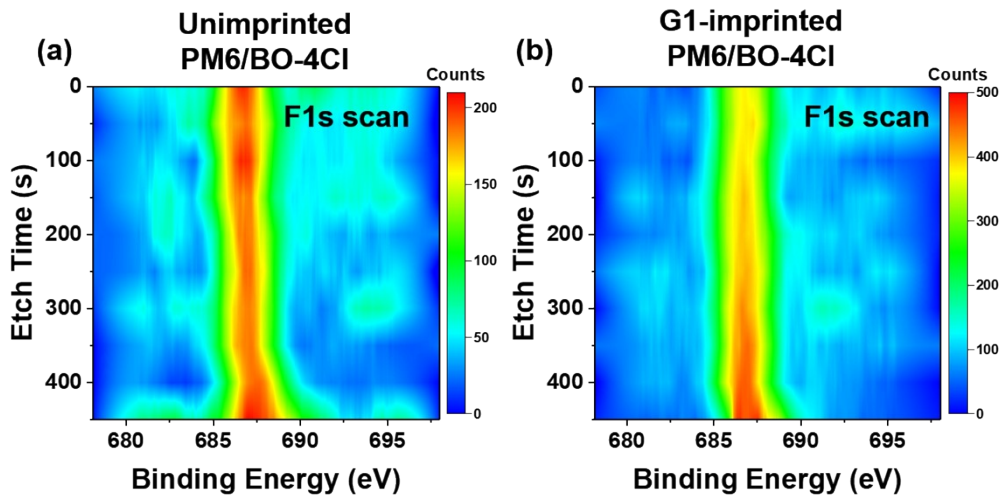

Figure S19. Dynamic X-ray photoelectron spectroscopy (DXPS) spectra (active layer region, F1s scan) of PM6/BO-4Cl films with (a) unimprinted PM6, and (b) G1-imprinted PM6.

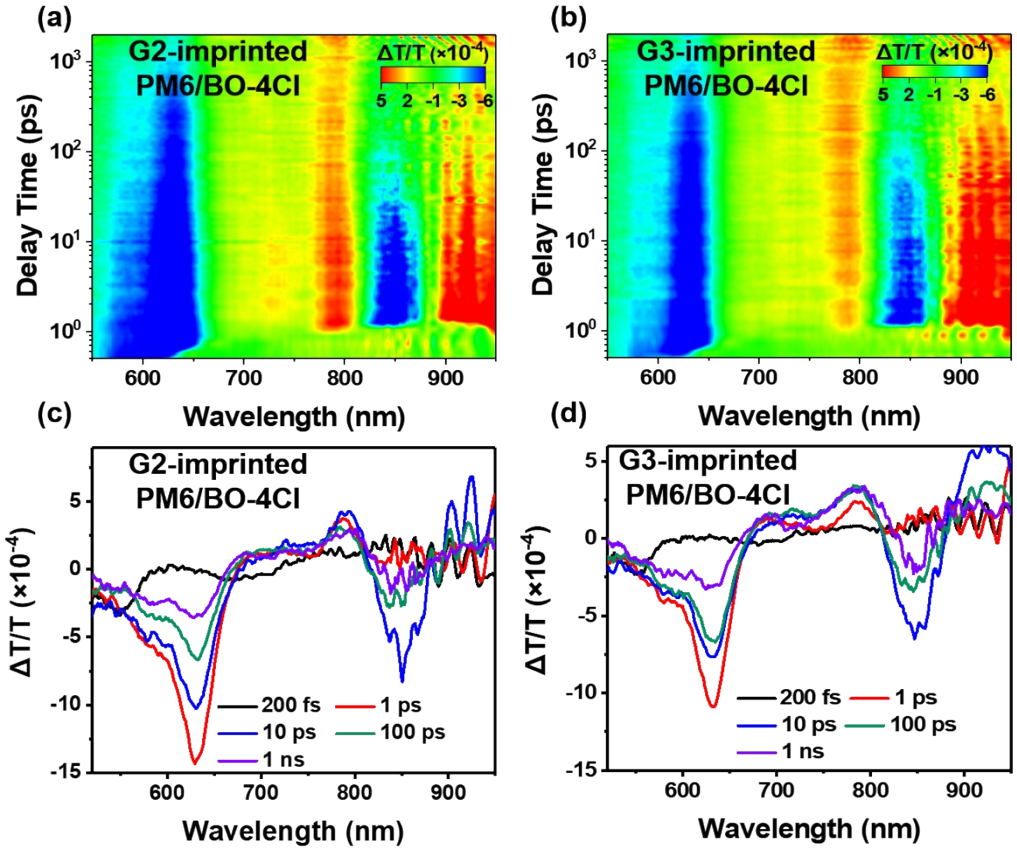

Figure S20. (a, b) TA images, (c, d) the corresponding TA spectra recorded at different delay times of PM6/BO-4Cl films with G2-imprinted PM6 and G3-imprinted PM6.

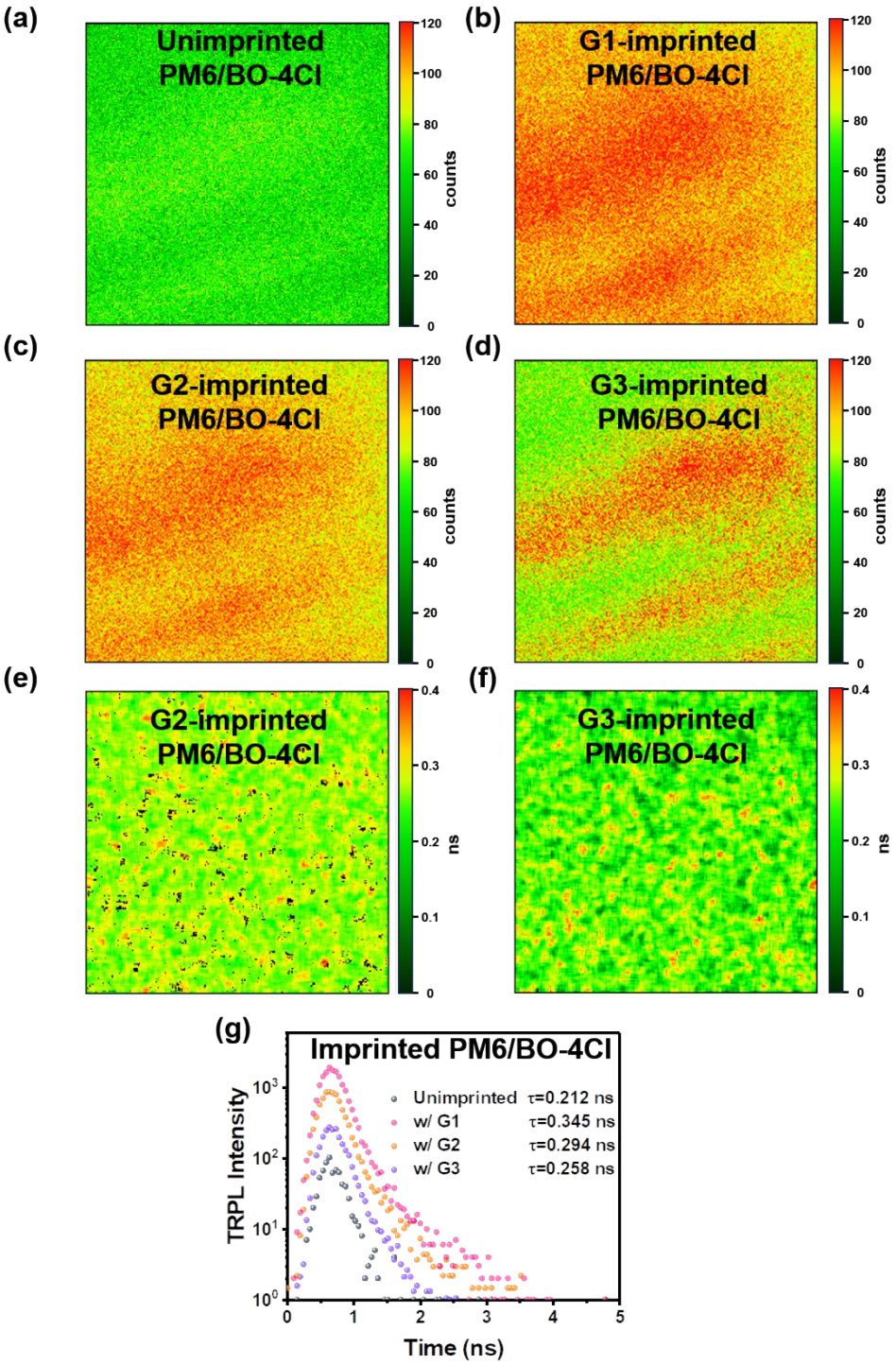

Figure S21. (a-d) Photoluminescence results of unimprinted and imprinted PM6/BO-4Cl films with different micropatterns. (e, f) Lifetime images, and (g) time-resolved photoluminescence (TRPL) decay profiles of lifetime imaging results of unimprinted and imprinted PM6/BO-4Cl films with different micropatterns.

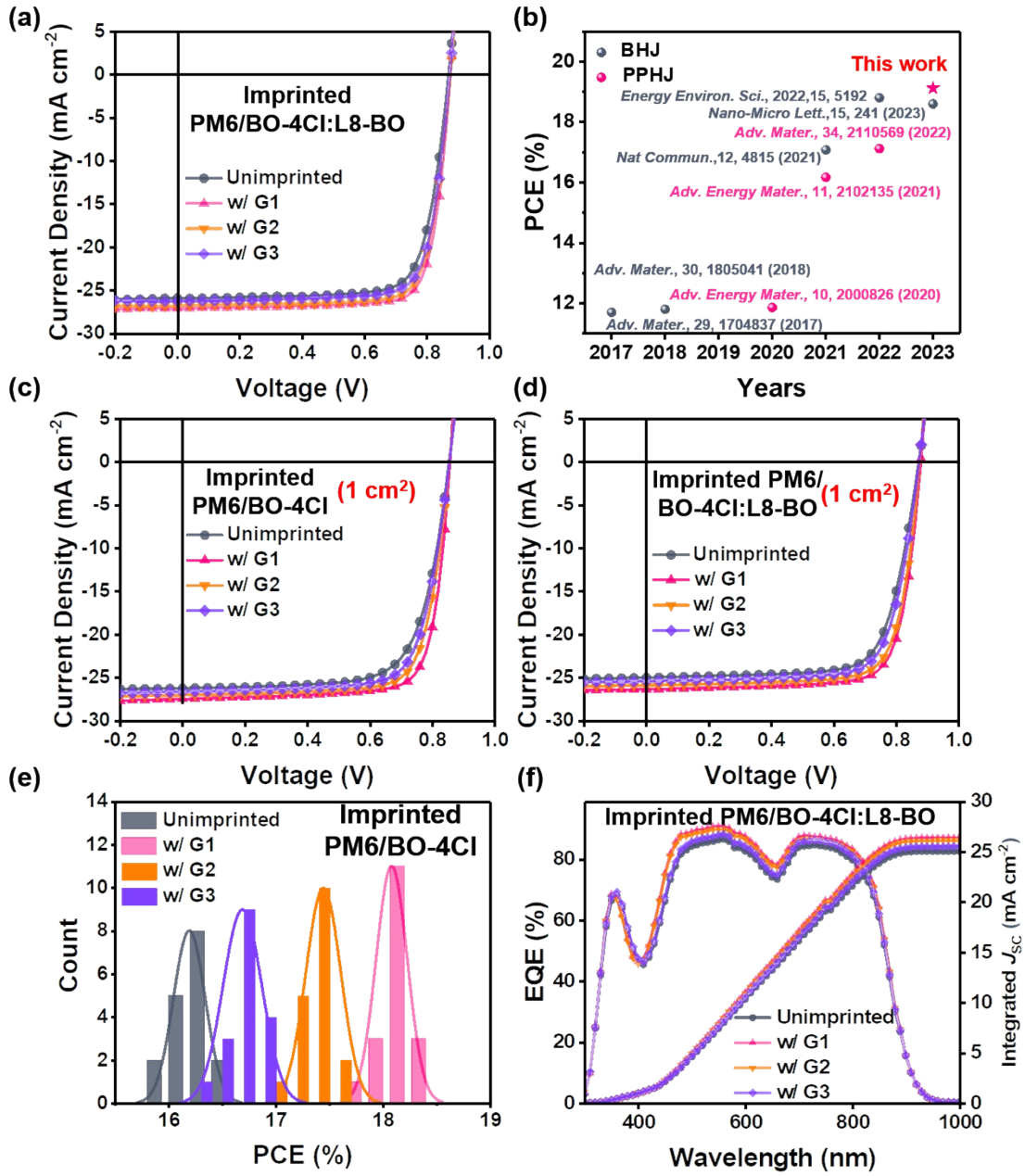

Figure S22. (a) *J-V* characteristics of PM6/BO-4Cl:L8-BO based on unimprinted and imprinted PM6/BO-4Cl films with different micropatterns. (b) Summary of PCE versus BHJ and PPHJ OSCs (0.04 cm^2) based on blade-coating process in other literature and in the present work. (c, d) *J-V* characteristics of PPHJ OSCs (1 cm^2) for PM6/BO-4Cl, and PM6/BO-4Cl:L8-BO, (e) histogram of the PCEs about 20 devices, (f) EQE spectra of PPHJ OSCs under simulated AM 1.5 G irradiation (100 mW cm^{-2}) based on unimprinted and imprinted PM6/BO-4Cl:L8-BO films with different micropatterns.

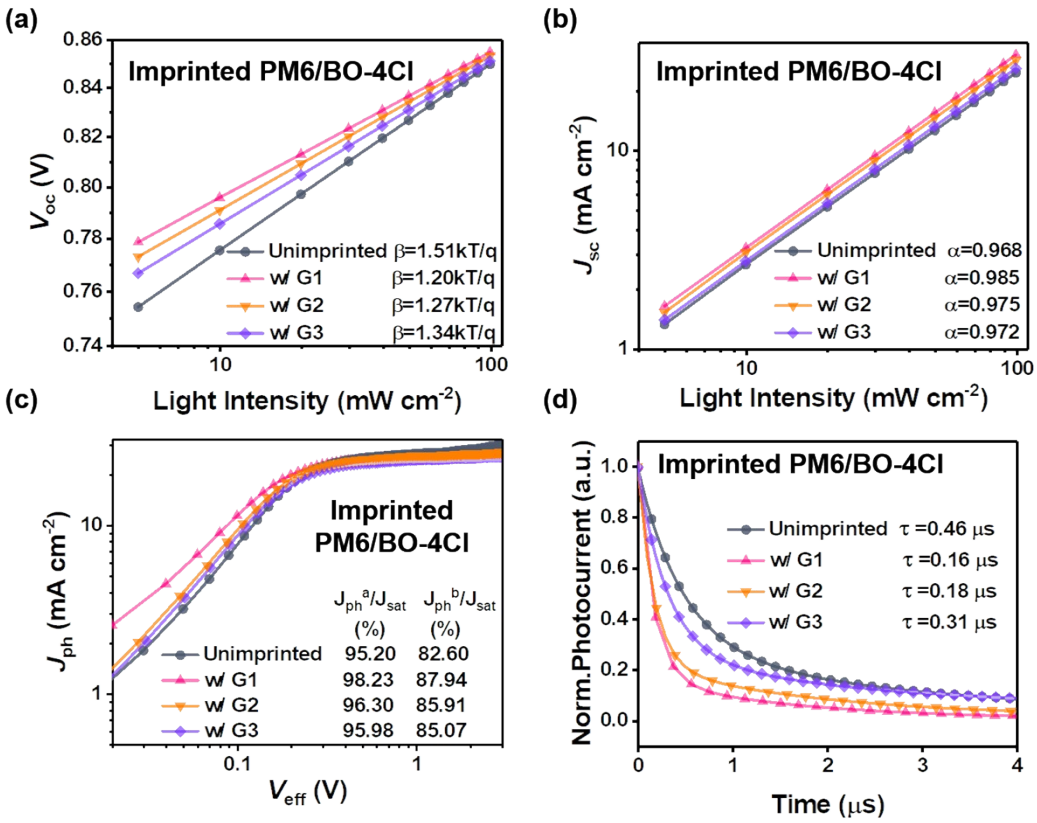

Figure S23. (a) V_{oc} versus light intensity, (b) J_{sc} versus light intensity, (c) J_{ph} - V_{eff} curves, (d) normalized transient photovoltage spectra of PPHJ OSCs based on unimprinted and imprinted PM6/BO-4Cl films with different micropatterns.

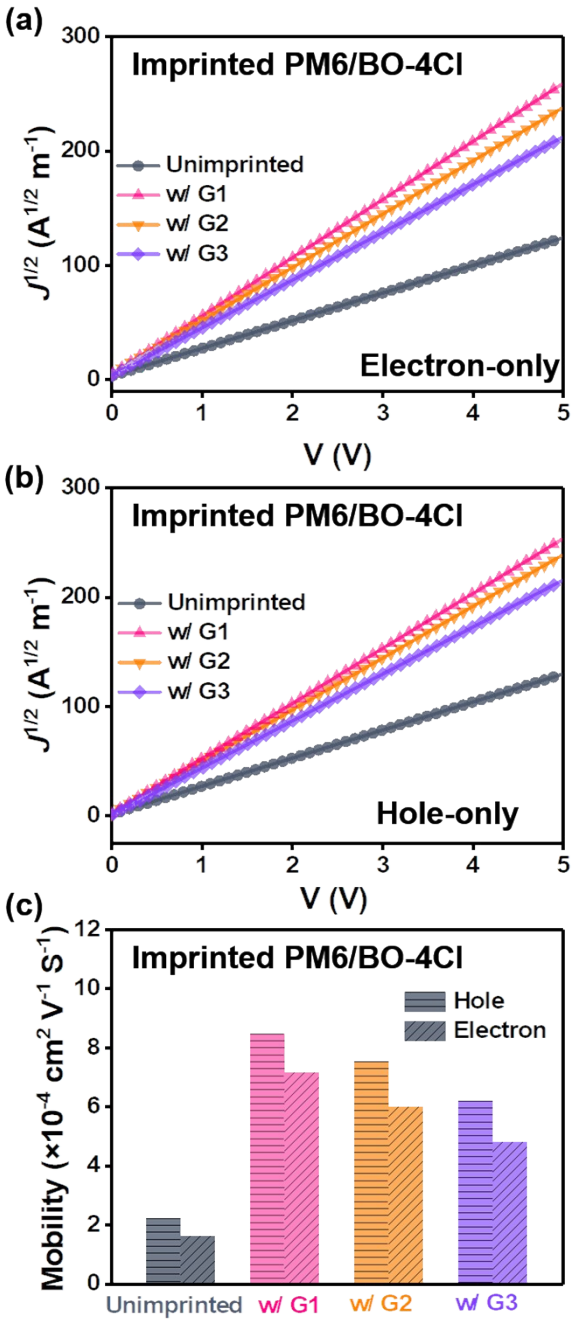

Figure S24. (a) Hole mobility with the structure of ITO/PEDOT:PSS/PM6/BO-4Cl/MoO_3/Ag, (b) electron mobility with the structure of ITO/ZnO/PM6/BO-4Cl/PDINN/Ag based on the SCLC method. (c) Carrier mobilities histogram of hole and electron mobilities of PPHJ OSCs based on unimprinted and imprinted PM6/BO-4Cl films with different patterns.

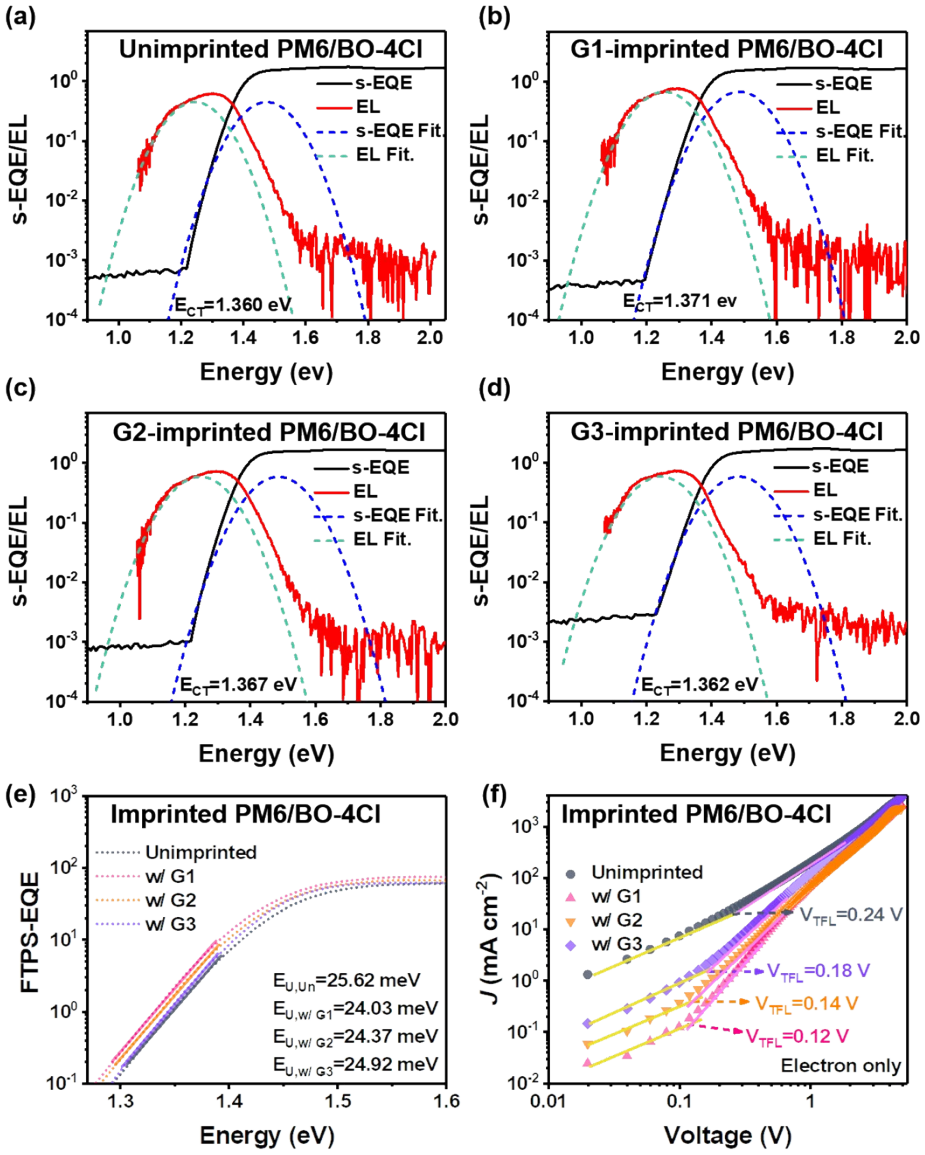

Figure S25. (a-d) Characterization of the CT state by simultaneously fitting of the sensitive-EQE and EL spectrum, and (e) Fourier transform photocurrent and EQE_{EL} (FTPS-EQE) spectra of the corresponding devices. (f) Dark current characteristics of the electron-only devices for trap density analysis of PPHJ OSCs based on unimprinted and imprinted PM6/BO-4Cl films with different micropatterns.

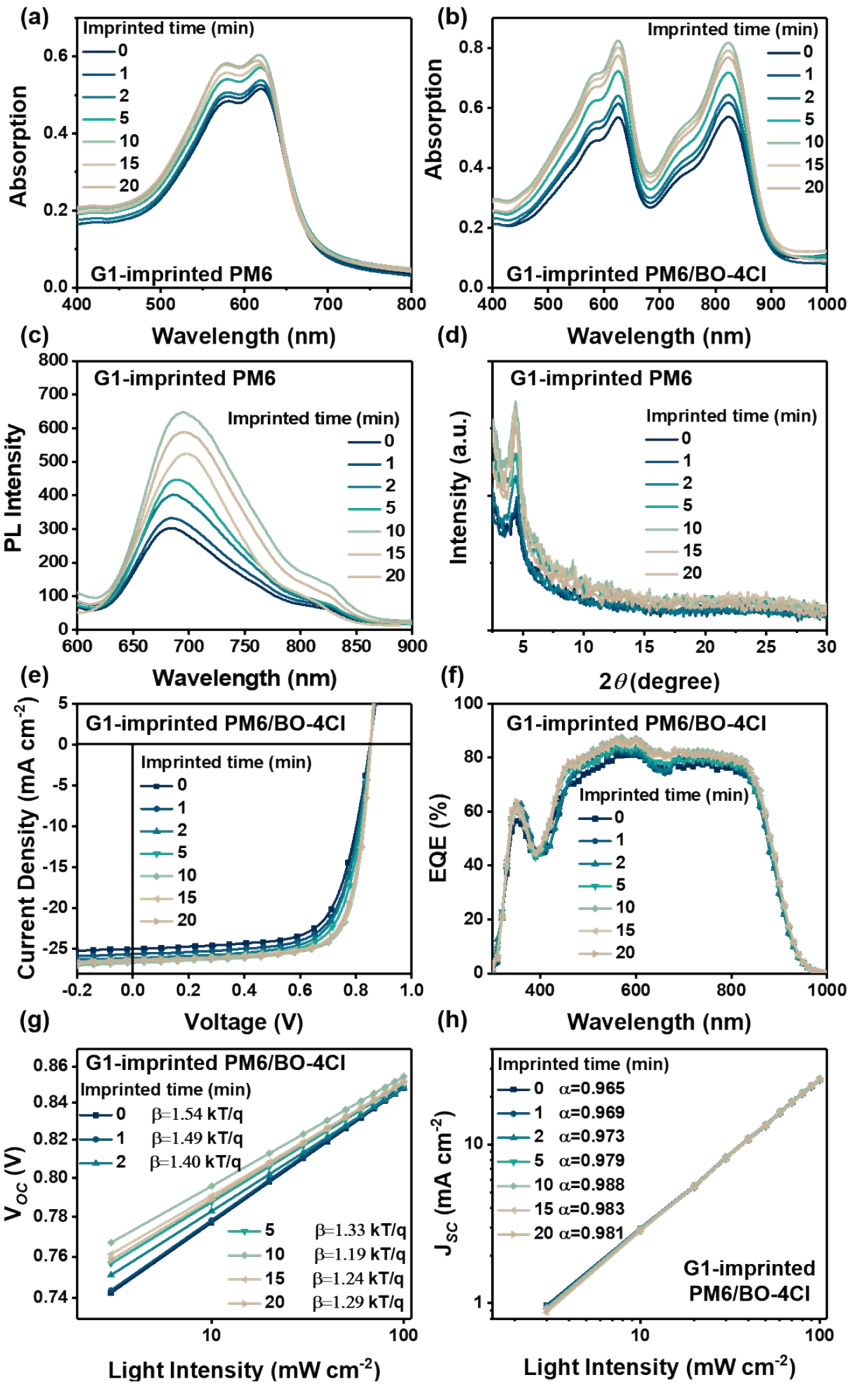

Figure S26. UV-vis absorption spectra of (a) PM6 and (b) PM6/BO-4Cl, (c) PL spectra, and (d) XRD patterns of PM6 films, (e) *J-V* characteristics and (f) the corresponding EQE spectra for PPHJ OSCs under simulated AM 1.5 G irradiation (100 mW cm^{-2}), (g) V_{oc} versus light intensity and (h) J_{sc} versus light intensity of devices with G1-imprinted PM6 at different imprinted time.

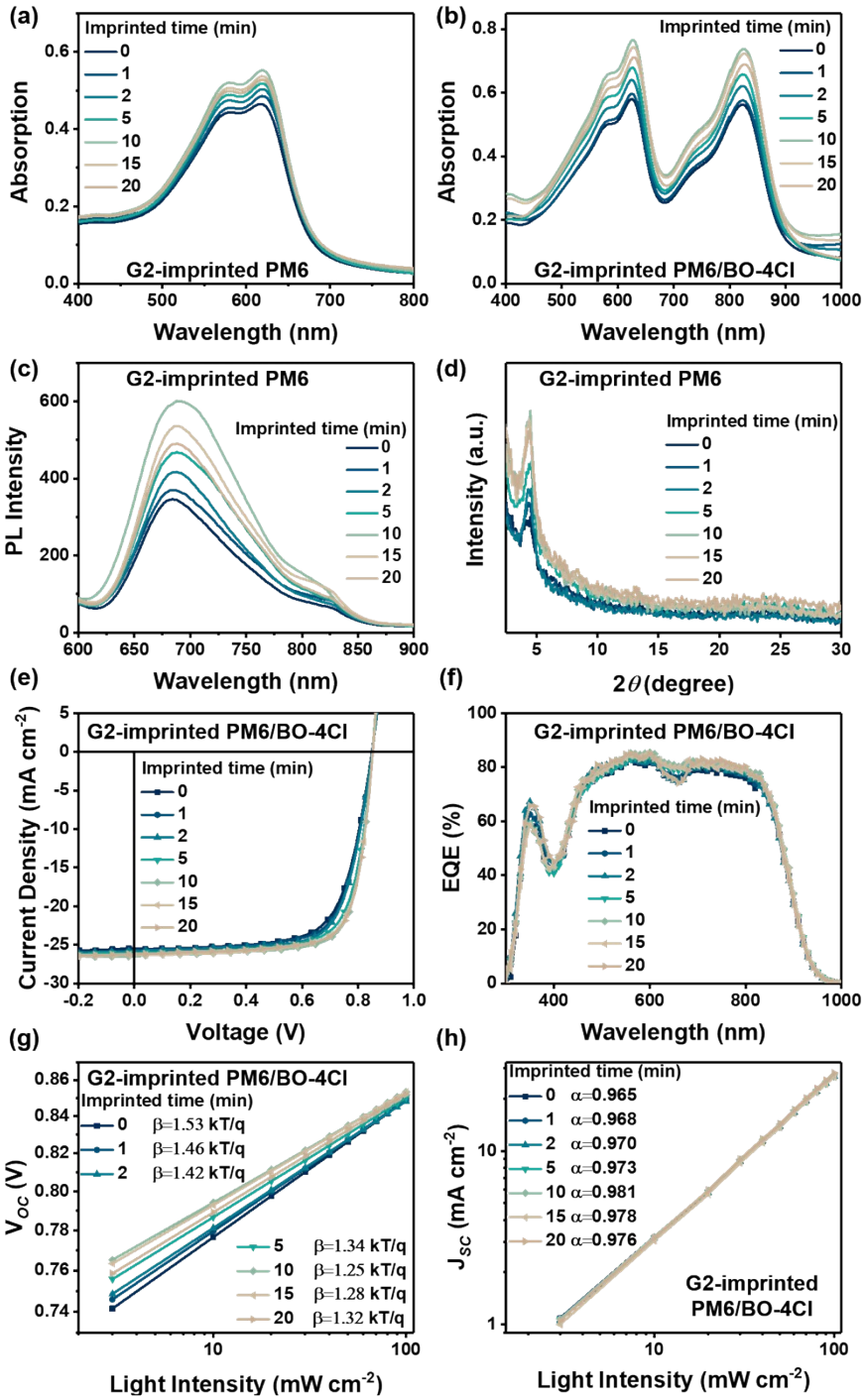

Figure S27. UV-vis absorption spectra of (a) PM6 and (b) PM6/BO-4Cl, (c) PL spectra, and (d) XRD patterns of PM6 films, (e) *J*-*V* characteristics and (f) the corresponding EQE spectra for PPHJ OSCs under simulated AM 1.5 G irradiation (100 mW cm^{-2}), (g) V_{oc} versus light intensity and (h) J_{sc} versus light intensity of devices with G2-imprinted PM6 at different imprinted time.

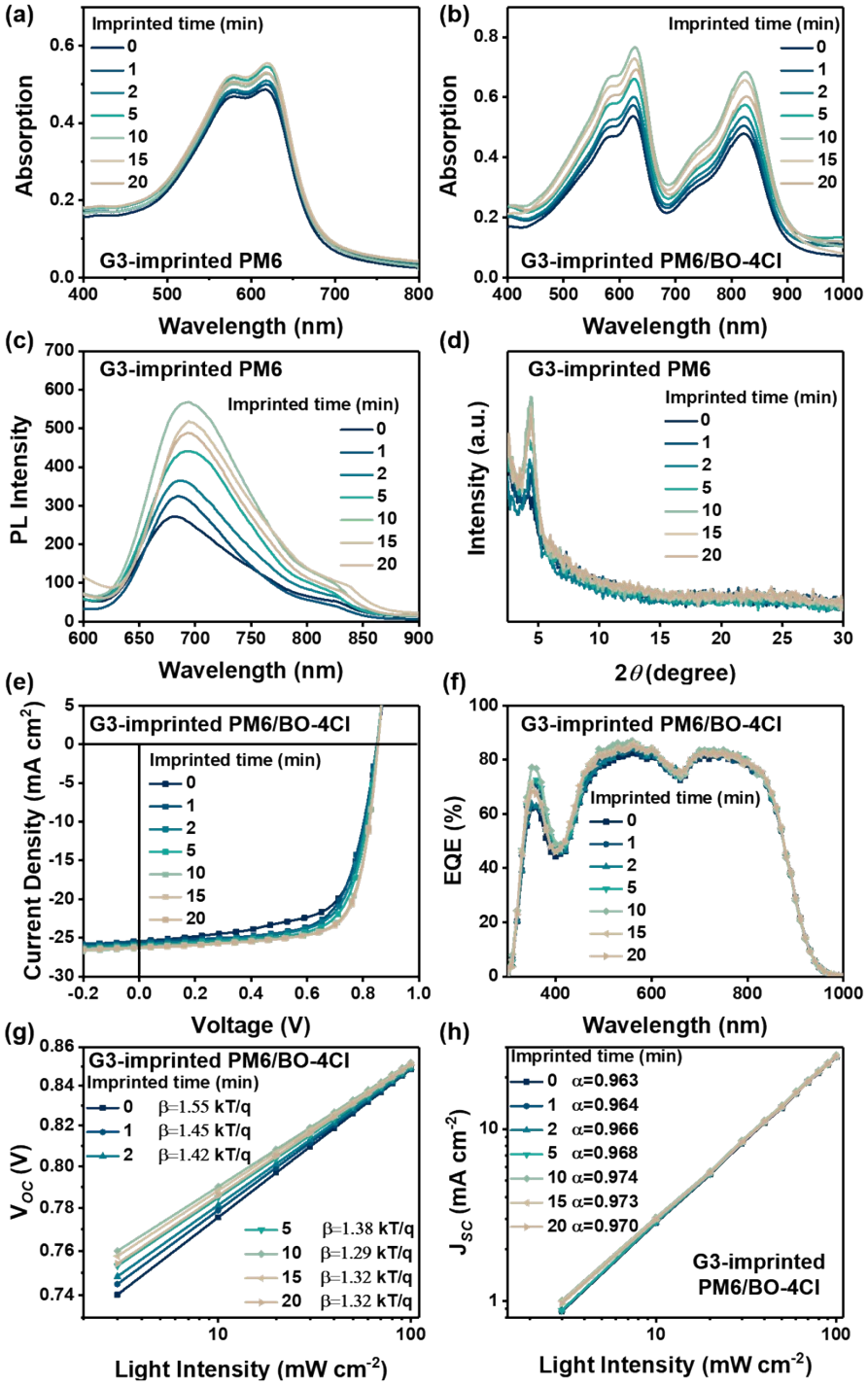

Figure S28. UV-vis absorption spectra of (a) PM6 and (b) PM6/BO-4Cl, (c) PL spectra, and (d) XRD patterns of PM6 films, (e) *J*-*V* characteristics and (f) the corresponding EQE spectra for PPHJ OSCs under simulated AM 1.5 G irradiation (100 mW cm^{-2}), (g) V_{oc} versus light intensity and (h) J_{sc} versus light intensity of devices with G3-imprinted PM6 at different imprinted time.

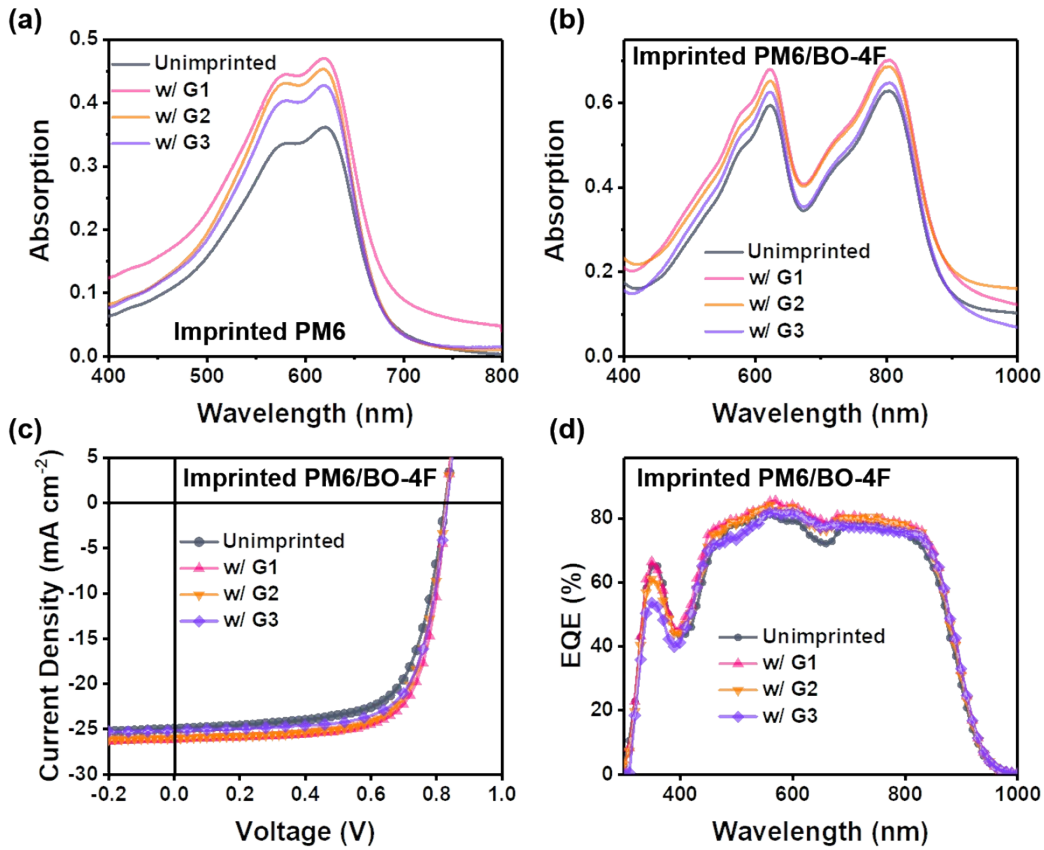

Figure S29. UV-vis absorption spectra of (a) PM6 and (b) PM6/BO-4F, (c) *J-V* characteristics and (d) the corresponding EQE spectra for PPHJ OSCs under simulated AM 1.5 G irradiation (100 mW cm^{-2}) based unimprinted PM6 and imprinted PM6 with different micropatterns.

Table S1. Crystal Coherence lengths (CCL) of (100) and (010) peaks and the d-spacing of unimprinted PM6 and imprinted PM6 with different micropatterns.

Direction / PM6	Out-of-plane				In-plane			
	π-π stacking cell axis (010)				Unit cell long axis (100)			
	q ($Å^{-1}$)	d-spacing (Å)	FWHM ($Å^{-1}$)	CCL (Å)	q ($Å^{-1}$)	d-spacing (Å)	FWHM ($Å^{-1}$)	CCL (Å)
-	1.649	3.810	0.400	15.71	0.285	22.059	0.104	54.39
w/ G1	1.667	3.769	0.318	19.76	0.322	19.358	0.070	81.08
w/ G2	1.664	3.775	0.331	18.98	0.325	19.506	0.073	77.64
w/ G3	1.667	3.769	0.347	18.11	0.289	21.758	0.088	64.08

Table S2. Summary of contact angle and surface energy of H_2O and CH_2I_2 based on PM6 and PM6/BO-4Cl with unimprinted PM6 and imprinted PM6 with different micropatterns.

Samples	Micropatterns	Contact angle		Surface energy (mN/m)
		θwater (°)	θCH_2I_2 (°0	
Imprinted PM6	-	101.33	46.84	36.74
	w/ G1	105.71	52.90	34.17
	w/ G2	105.41	50.08	34.73
	w/ G3	104.48	48.90	35.05
Imprinted PM6/BO-4Cl	-	95.66	44.32	40.80
	w/ G1	102.07	50.28	36.21
	w/ G2	100.52	46.95	38.09
	w/ G3	99.51	44.95	39.24

Table S3. CCL of the (100) and (010) peaks and the d-spacing of PM6/BO-4Cl with unimprinted PM6 and imprinted PM6 by different micropatterns, respectively.

Direction / PM6	Out-of-plane				In-plane			
	π-π stacking cell axis (010)				Unit cell long axis (100)			
	q ($Å^{-1}$)	d-spacing (Å)	FWHM ($Å^{-1}$)	CCL (Å)	q ($Å^{-1}$)	d-spacing (Å)	FWHM ($Å^{-1}$)	CCL (Å)
-	1.761	3.562	0.535	11.74	0.294	21.371	0.151	41.61
w/ G1	1.805	3.481	0.381	16.49	0.308	20.400	0.069	91.06
w/ G2	1.792	3.506	0.404	15.55	0.301	20.874	0.089	70.60
w/ G3	1.769	3.552	0.509	12.34	0.298	21.085	0.140	44.88

Table S4. Summary of photovoltaic parameters for large-area (1 cm^2) PPHJ OSCs based on PM6/BO-4Cl system with unimprinted PM6 and imprinted PM6 by different micropatterns under the AM 1.5 G condition.

System	Micropattern	V_{oc} (V)	J_{sc} (mA/cm^2)	FF (%)	PCE (%)
Imprinted PM6/BO-4Cl	-	0.852	25.04	71.95	15.34
	w/ G1	**0.856**	**26.22**	**78.07**	**17.52**
	w/ G2	0.855	25.84	76.30	16.86
	w/ G3	0.853	25.41	74.04	16.04
Imprinted PM6/BO-4Cl:L8-BO	-	0.872	24.97	73.92	16.09
	w/ G1	**0.877**	**26.41**	**77.65**	**17.98**
	w/ G2	0.875	25.98	76.94	17.49
	w/ G3	0.873	25.47	74.65	16.59

Table S5. BHJ and PPHJ OSCs PCEs based on blade-coating process in other literature and this work.

Structure	Films	PCE (%)	Reference
BHJ	PBTA-TF:IT-M	11.70	1
	PBDB-T:FOIC:PTB7-Th	11.80	2
	PM6:BTP-eC9	17.48	3
	PM1:L8-BO:BTP-F3Cl	18.80	4
	PM6:L8-BO: YDT-SeNF	18.60	5
PPHJ	PBDB-T: FOIC /IT-M:IT-M	11.86	6
	PM6/Y6	16.17	7
	PM6/BTP-BO-4Cl	17.12	8
	PM6/BO-4Cl	18.47	This work
	PM6/BO-4Cl:L8-BO	19.12	

Table S6. The parameter of charge collection and exciton dissociation of PPHJ OSCs based on PM6/BO-4Cl system with unimprinted PM6 and imprinted PM6 by different micropatterns, respectively.

Imprinted PM6/BO-4Cl	J_{sat} （mA cm^{-2})	$J_{ph}{}^{a}$ （mA cm^{-2})	$J_{ph}{}^{b}$ (mA cm^{-2})	$J_{ph}{}^{a}/J_{sat}$ (%)	$J_{ph}{}^{b}/J_{sat}$ (%)
-	25.35	24.13	20.94	95.20	82.60
w/ G1	26.23	25.77	23.07	98.23	87.94
w/ G2	25.64	24.69	22.03	96.30	85.91
w/ G3	25.52	24.49	21.71	95.98	85.07

Table S7. The hole and electron mobilities of PPHJ OSCs based on PM6/BO-4Cl system with unimprinted PM6 and imprinted PM6 by different micropatterns, respectively.

Imprinted PM6/BO-4Cl	μ_h ($\times10^{-4}$ cm^2 V^{-1} S^1)	μ_e ($\times10^{-4}$ cm^2 V^{-1} S^1)	μ_h/μ_e
-	2.21	1.61	1.37
w/ G1	8.47	7.16	1.19
w/ G2	7.52	5.99	1.26
w/ G3	6.19	4.80	1.29

Table S8. Summary of photovoltaic parameters for OSCs based on PM6/BO-4Cl system imprinted with different micropatterns at different imprinted time under the AM 1.5 G condition.

Imprinted PM6/BO-4Cl	Imprint Time (min)	J_{sc} (mA/cm^2)	V_{oc} (V)	FF (%)	PCE (%)
w/ G1	0	25.60	0.850	74.31	16.17
	1	25.95	0.850	75.57	16.67
	2	26.11	0.851	77.68	17.26
	5	26.43	0.852	77.78	17.51
	10	**26.80**	**0.854**	**79.23**	**18.13**
	15	26.56	0.852	78.95	17.87
	20	26.49	0.852	78.62	17.74
w/ G2	0	25.53	0.850	74.70	16.21
	1	25.72	0.850	76.25	16.67
	2	25.84	0.851	77.08	16.95
	5	26.03	0.852	77.82	17.26
	10	**26.45**	**0.853**	**78.41**	**17.69**
	15	26.34	0.852	78.21	17.55
	20	26.19	0.852	78.05	17.41
w/ G3	0	25.43	0.850	74.21	16.04
	1	25.54	0.850	74.33	16.13
	2	25.71	0.850	74.68	16.32
	5	25.86	0.851	75.14	16.54
	10	**26.17**	**0.852**	**75.90**	**16.92**
	15	26.11	0.852	75.83	16.86
	20	26.05	0.851	75.74	16.79

Table S9. Summary of photovoltaic parameters for OSCs based on PM6 (TL solution)/BO-4F (THF solution) system with unimprinted PM6 and imprinted PM6 by different micropatterns under the AM 1.5 G condition.

Imprinted PM6/BO-4F	V_{oc} (V)	J_{sc} (mA/cm^2)	FF (%)	PCE (%)
-	0.835	25.07	68.99	14.44
w/ G1	**0.836**	**26.18**	**72.04**	**15.70**
w/ G2	0.835	25.74	71.21	15.31
w/ G3	0.834	25.22	70.90	14.91

Reference

1. W. Zhao, S. Zhang, Y. Zhang, S. Li, X. Liu, C. He, Z. Zheng and J. Hou, *Adv. Mater.,* 2018, **30**, 1704837.
2. L. Zhang, X. Xu, B. Lin, H. Zhao, T. Li, J. Xin, Z. Bi, G. Qiu, S. Guo, K. Zhou, X. Zhan and W. Ma, *Adv. Mater.,* 2018, **30**, 1805041.
3. Y. Zhang, K. Liu, J. Huang, X. Xia, J. Cao, G. Zhao, P. W. K. Fong, Y. Zhu, F. Yan, Y. Yang, X. Lu and G. Li, *Nat. Commun.,* 2021, **12**; 4815.
4. J. Wan, Y. Wu, R. Sun, J.-W. Qiao, X.-T. Hao and J. Min, *Energy Environ. Sci.,* 2022, **15**, 5192.
5. H. Bai, R. Ma, W. Su, T. A. D. Peña, T. Li, L. Tang, J. Yang, B. Hu, Y. Wang, Z. Bi, Y. Su, Q. Wei, Q. Wu, Y. Duan, Y. Li, J. Wu, Z. Ding, X. Liao, Y. Huang, C. Gao, G. Lu, M. Li, W. Zhu, G. Li, Q. Fan and W. Ma, *Nano-Micro Lett.,* 2023, **15**, 241.
6. Y. Wang, X. Wang, B. Lin, Z. Bi, X. Zhou, H. B. Naveed, K. Zhou, H. Yan, Z. Tang and W. Ma, *Adv. Energy Mater.,* 2020, **10**, 2000826.
7. Y. Zheng, R. Sun, M. Zhang, Z. Chen, Z. Peng, Q. Wu, X. Yuan, Y. Yu, T. Wang, Y. Wu, X. Hao, G. Lu, H. Ade and J. Min, *Adv. Energy Mater.,* 2021, **11**, 2102135.
8. J. Fan, Z. Liu, J. Rao, K. Yan, Z. Chen, Y. Ran, B. Yan, J. Yao, G. Lu, H. Zhu, C. Li and H. Chen, *Adv. Mater.,* 2022, **34**, 2110569.